

---

# AMORTIZED BAYESIAN MULTILEVEL MODELS

---

**Daniel Habermann**  
Department of Statistics  
TU Dortmund University  
Germany

**Marvin Schmitt**  
Cluster of Excellence SimTech  
University of Stuttgart  
Germany

**Lars Kühmichel**  
Department of Statistics  
TU Dortmund University  
Germany

**Andreas Bulling**  
Institute for Visualisation and Interactive Systems  
University of Stuttgart  
Germany

**Stefan T. Radev**  
Department of Cognitive Science  
Rensselaer Polytechnic Institute  
USA

**Paul-Christian Bürkner**  
Department of Statistics  
TU Dortmund University  
Germany

## ABSTRACT

Multilevel models (MLMs) are a central building block of the Bayesian workflow. They enable joint, interpretable modeling of data across hierarchical levels and provide a fully probabilistic quantification of uncertainty. Despite their well-recognized advantages, MLMs pose significant computational challenges, often rendering their estimation and evaluation intractable within reasonable time constraints. Recent advances in simulation-based inference offer promising solutions for addressing complex probabilistic models using deep generative networks. However, the utility and reliability of deep learning methods for estimating Bayesian MLMs remains largely unexplored, especially when compared with gold-standard samplers. To this end, we explore a family of neural network architectures that leverage the probabilistic factorization of multilevel models to facilitate efficient neural network training and subsequent near-instant posterior inference on unseen data sets. We test our method on several real-world case studies and provide comprehensive comparisons to Stan as a gold-standard method where possible. Finally, we provide an open-source implementation of our methods to stimulate further research in the nascent field of amortized Bayesian inference.

**Keywords** Bayesian Models, Amortized Inference, Multilevel Models

## 1 Introduction

Obtaining accurate inference and faithful uncertainty quantification in reasonable time is a frontier of today’s statistical research (Cranmer et al., 2020). One major difficulty arising in most experimental and almost all observational data is the presence of complex dependency structures, for example, due to natural groupings (e.g., data gathered in different countries) or repeated measurements of the same observational units over time (e.g., particles, bacteria, or people; Gelman and Hill, 2006). To leverage these dependency structures, multilevel models (MLMs), also referred to as latent variable, hierarchical, random, or mixed effects models, have become an integral part of modern Bayesian statistics (Goldstein, 2011; Gelman et al., 2013; McGlothlin and Viele, 2018; Finch et al., 2019; Yao et al., 2022).

Despite the wide success of Bayesian MLMs across the quantitative sciences, a major challenge is their limited efficiency and scalability when dealing with large and complex data. This is because estimating the full posterior distribution of all parameters of interest can be very costly (Gelman et al., 2013). For models where the likelihood function is analytically tractable and differentiable with respect to model parameters, Markov chain Monte Carlo (MCMC) sampling algorithms

as implemented in probabilistic programming languages like Stan (Stan Development Team, 2024) are the current gold standard for generating accurate draws from the posterior distribution.

Considerable effort has been made to improve the sampling speed of MCMC algorithms, especially for high-dimensional models with rich structure, such as MLMs. This includes step-size adjustments or reparameterizations to work-around or improve the posterior geometry (Hoffman et al., 2019; Modi et al., 2023), enabling within-chain parallelization via parallel evaluation of the likelihood (Stan Development Team, 2024), as well as the development of specialized algorithms that entail faster and more reliable adaptation phases, such that multiple shorter chains can be run in parallel (Zhang et al., 2022; Margossian et al., 2021). However, despite these advancements, sampling methods based on MCMC are still too slow for many multilevel settings. Even for models and data sets of moderate size, posterior inference can take days or even weeks, creating a large gap between the models that researchers might want to compute and the models that are computationally feasible. Expanding the space of models that can be fit in a reasonable time frame is therefore an important requirement for the broad applicability of Bayesian MLMs.

In addition to sampling speed, there are two fundamental issues with posterior inference for Bayesian MLMs in most applications of scientific interest:

1. The need to rerun computationally expensive sampling algorithms when new data becomes available or when computational faithfulness needs to be assessed;
2. Efficient sampling for models with high-dimensional and highly structured, intractable or non-differentiable likelihoods.

Issue (1) is a crucial limiting factor in cases where data are arriving in real-time or many datasets need to be evaluated. In addition, essential steps in the modern Bayesian workflow (Gelman et al., 2020) like cross-validation (Vehtari et al., 2017; Merkle et al., 2019) or simulation-based calibration (SBC, Talts et al., 2018; Modrák et al., 2023) require many model refits on subsets of the data, rendering careful model testing a time-intensive task for all but the simplest models. Issue (2) is also becoming increasingly common, as many scientific domains nowadays employ models whose output is the result of a complex simulation program (Cranmer et al., 2020). Consequently, closed-form solutions for the likelihood are often unavailable.

Both of these issues have led to the development of novel algorithms that do not rely on MCMC sampling. For models without a tractable likelihood, simulation-based inference methods like approximate Bayesian computation (ABC, Sisson et al., 2018) can sample from the posterior without computing the likelihood directly. The main drawback of ABC is that it heavily suffers from the curse of dimensionality (Barber et al., 2015) as the number of parameters increases. This is of particular concern for MLMs as their number of parameters scales linearly with the number of groups in the data. While ABC algorithms for MLMs have been developed (Sisson and Fan, 2011), they have not managed to fully overcome this major drawback of ABC. Other approaches to Bayesian inference for MLMs with intractable likelihoods include mean-field variational algorithms (Tran et al., 2017; Roeder et al., 2019), but this class of algorithms suffers from significant loss of accuracy in posterior estimation (Yao et al., 2018).

Recently, algorithms based on neural density estimation have shown to be promising alternatives to classical MCMC. One particular advantage of neural density estimation (Papamakarios and Murray, 2016) is that it allows to sample from the posterior conditioned on data samples of any size almost immediately after an initial training phase (Radev et al., 2020). This property is called *amortization* (Gershman and Goodman, 2014), as the initial time investment during training amortizes at inference time by allowing posterior inference for new data sets typically within a fraction of a second. Additionally, this new class of neural simulation-based algorithms scales to high-dimensional models and can naturally deal with models lacking tractable likelihoods (Cranmer et al., 2020). Neural density estimators emulate sampling from an intractable distribution via neural networks that transform a random input vector into a draw from a target probability distribution. By using training examples of the joint (Bayesian) model  $p(\mathbf{x}, \boldsymbol{\theta})$ , they can generate approximate draws from the posterior distribution  $p(\boldsymbol{\theta} | \mathbf{x})$ . Importantly, the neural networks are only used to sample from the posterior of an underlying Bayesian model and are not used for fitting the data directly. Methods building on neural posterior density estimation have shown tremendous success in performing inference for complex and otherwise intractable models in different applications like neuroscience (Gonçalves et al., 2020), cognitive science (Radev et al., 2020), epidemiology (Radev et al., 2021), psychology (von Krause et al., 2022), medicine (Wehenkel et al., 2023), physics (Brehmer et al., 2020), and engineering (Zhang and Mikelsons, 2023). Yet, fully amortized Bayesian inference is still a developing field.

One of the current major challenges for amortized Bayesian inference lies in efficiently capturing complex dependencies. Such dependency structures are for example encountered in global-local shrinkage priors (Piironen and Vehtari, 2017), item response theory models (Bürkner, 2021), longitudinal studies (Steele, 2008), and in many other settings where MLMs are applied (Gelman and Hill, 2006). The fundamental statistical assumption of MLMs is that a set of parameters, defined according to the hierarchical structure of the data, are *exchangeable* and originate from the same underlying

distribution whose hyper-parameters are subsequently estimated from the data. In this aspect, they are particularly suitable for data with complex dependency structures: Instead of inferring estimates for each group in isolation (*no pooling*) or disregarding the grouping structure of the data (*complete pooling*), MLMs can capture similarities across groups while also allowing for group-level variation. This *partial-pooling* property increases the robustness of the obtained parameter estimates, helps to ensure their accurate uncertainty calibration, and improves predictive performance (Gelman, 2006).

Expanding neural density estimation to MLMs is challenging because the dimension of the posterior depends on the number of groups and may vary over data sets. Such a setting requires bespoke neural architectures to lift the requirement of fixed-length inputs. Amortized inference with varying group sizes in MLMs is complicated by the fact that estimates of local parameters for one group depend not only on that specific group but also on all other groups in the dataset. Additionally, the number of parameters increases linearly with the number of groups, rendering network training inefficient for data sets with a large number of groups.

In important pioneering work, initial progress has been made to address these challenges (Rodrigues et al., 2021; Arruda et al., 2023; Heinrich et al., 2023), but they have so far considered only a narrow range of MLMs and have performed only limited validation against state-of-the-art Bayesian samplers. In particular, existing methods do not consider (1) simultaneous amortization over both the number of groups and the number of observations per group, (2) amortization over spaces of covariates, (3) simultaneous joint estimation with non-IID response variables, (4) highly correlated group-level parameters, (5) additional (non-hierarchical) shared parameters, (6) systematic calibration and shrinkage analysis to verify inference correctness at each level, as well as (7) discussing different neural factorizations that equivalently follow from the same probabilistic model structure. Our proposed framework addresses all of these challenges by making the following key contributions:

- We develop neural network architectures that utilize the probabilistic factorization of the likelihood of multilevel models to facilitate efficient neural network training and subsequent near-instant amortized posterior inference.
- We test our method on a wide range of real-world case studies together covering all the above mentioned challenges. We also provide comparisons to Stan as a gold-standard method for posterior inference whenever possible.
- We provide an efficient and user-friendly implementation of our algorithm in the BayesFlow Python library (Radev et al., 2023b). In this way, users can benefit from amortized inference for otherwise intractable models and generate fast and accurate draws from the posterior distribution.

## 2 Methods

Below, we review the several components that together enable fully amortized Bayesian inference on multilevel models. The novel methodological contributions of this paper start from Subsection 2.4.

### 2.1 Notation and Definitions

Following Robert et al. (2007), we consider parametric Bayesian models defined by a joint distribution  $p(\boldsymbol{\theta}, \mathbf{x})$  over all random quantities in an application domain of interest. We assume that  $\boldsymbol{\theta} \in \mathbb{R}^D$  represents all unobservable (latent) quantities, whereas  $\mathbf{x} \in \mathcal{X}$  denotes all observable (manifest) quantities. We also assume that the joint distribution factorizes into a likelihood  $p(\mathbf{x} | \boldsymbol{\theta})$  and a prior  $p(\boldsymbol{\theta})$ , defining a “generative model” that can be translated into a computer program and “sampled” according to a simple ancestral scheme:

$$\boldsymbol{\theta} \sim p(\boldsymbol{\theta}) \tag{1}$$

$$\mathbf{x} \sim p(\mathbf{x} | \boldsymbol{\theta}) \tag{2}$$

Consequently, *multilevel models* emerge as a special case of this general formulation, prescribing an explicit and application-dependent factorization to the prior  $p(\boldsymbol{\theta})$ , for instance,  $p(\boldsymbol{\theta}) = p(\theta_1) p(\theta_2 | \theta_1) p(\theta_3 | \theta_2, \theta_1) \cdots p(\theta_D | \theta_{D-1}, \dots, \theta_1)$ . Ideally, the particular factorization reflects the probabilistic structure of the assumed data-generating process. For example, a two-level model assuming exchangeable groups and exchangeable observations within groups can be sampled according to

$$\theta_1 \sim p(\theta_1) \tag{3}$$

$$\theta_d \sim p(\theta_d | \theta_1) \quad \text{for } d = 2, \dots, D \tag{4}$$

$$\mathbf{x}_{nd} \sim p(\mathbf{x}_{nd} | \theta_d) \quad \text{for } n = 1, \dots, N_d \tag{5}$$

where the “hyperparameters”  $\theta_1$  are commonly denoted with their own symbol (e.g.,  $\tau$ ). The typical target of Bayesian analysis is then the *joint posterior* over all parameters

$$p(\theta_1, \dots, \theta_D | \mathbf{x}_{11}, \dots, \mathbf{x}_{DN_D}) \propto p(\theta_1) \prod_{d=2}^D p(\theta_d | \theta_1) \prod_{n=1}^{N_d} p(\mathbf{x}_{nd} | \theta_d), \quad (6)$$

which generally admits a non-unique factorization (Stuhlmüller et al., 2013) and is too complex to calculate analytically. Thus, MCMC algorithms, such as Gibbs (Gelfand, 2000) or Hamiltonian Monte Carlo (HMC) samplers (Neal, 2011) are commonly employed to approximate the posterior whenever the likelihood  $p(\mathbf{x} | \theta)$  is analytically tractable (e.g., when it follows a known density function). In recent years, *implicit models* (Diggle and Gratton, 1984) have gained considerable traction in scientific modeling. These models require novel *likelihood-free* or *simulation-based* methods that bypass the evaluation of the intractable likelihood (Cranmer et al., 2020).

## 2.2 Simulation-Based Inference

In scientific modeling, the likelihood  $p(\theta | \mathbf{x})$  of the model may often be analytically intractable, for example, because the model contains differential equations without known analytical solutions or several levels of latent variables following complex generative procedures (Diggle and Gratton, 1984; Cranmer et al., 2020). The Bayesian generative model is then only available as a triple of the prior  $p(\theta)$  over simulation parameters  $\theta$ , a probabilistic model  $p(\nu | \theta)$  for nuisance parameters (aka. noise)  $\nu$ , and a simulation program  $g : (\theta, \nu) \mapsto \mathbf{x}$  that outputs synthetic observable data  $\mathbf{x}$ . More concretely, the forward process is defined as

$$\mathbf{x} = g(\theta, \nu) \quad \text{with} \quad \nu \sim p(\nu | \theta), \quad \theta \sim p(\theta). \quad (7)$$

We can readily sample from this *generative model* and obtain pairs of observable data  $\mathbf{x}$  along with the data-generating parameters  $\theta$ . When estimating models with analytically intractable likelihoods, one commonly speaks of *likelihood-free inference*, a term that is somewhat misleading as the likelihood still *implicitly* exists as an integral over all possible execution paths (as represented by the stochastic noise variates  $\nu$ ),

$$p(\mathbf{x} | \theta) = \int p(\mathbf{x}, \nu | \theta) d\nu, \quad (8)$$

even though the analytic form of that likelihood  $p(\mathbf{x} | \theta)$  is generally unknown (Cranmer et al., 2020). Nevertheless, Monte Carlo simulations from the full model (Equation 7) can be cleverly used to perform fully Bayesian inference, which motivates the alternative and more descriptive term *simulation-based inference* (SBI). Intractable models that require SBI are ubiquitous in the quantitative sciences and SBI has been conceptualized as one of the key pillars of today’s computational stack (Lavin et al., 2021).

Simulation-based methods are also applicable when the likelihood is tractable, as is the case in many MLM applications. Traditionally, for tractable likelihood models, simulation-based methods were not considered because they were inferior to density-based inference methods (e.g., MCMC) in terms of both inference speed and accuracy. However, simulation-based training of neural networks seems crucial for achieving *amortized Bayesian inference* via neural networks (see below), regardless of whether we have access to the analytic likelihood (or prior) densities.

## 2.3 Amortized Bayesian inference

While performing Bayesian inference for high-dimensional models on a single data set is already challenging, the computational burden increases significantly when the same model must be applied to multiple data sets. Achieving accurate posterior inference can quickly become too computationally expensive in such cases. This issue is most apparent when fitting the same statistical model to several or sometimes millions (von Krause et al., 2022) of mutually independent data sets.

However, even with a single data set, numerous refits of the same model might be necessary. For example, established state-of-the-art model evaluation techniques require multiple model refits to different datasets or subsets. Two such methods in the Bayesian workflow (Gelman et al., 2020) are simulation-based calibration (SBC; Talts et al., 2018) and cross-validation (CV; Vehtari et al., 2017). While SBC can validate the approximation in the closed-world setting, CV evaluates its predictive out-of-sample performance (see Section 3 for more details). In Section 3.2, we show that amortized Bayesian inference can provide considerable speed advantages for these methods which comprise key steps in a principled Bayesian workflow (Gelman et al., 2020).

Amortized Bayesian Inference (ABI) (ABI; Gershman and Goodman, 2014; Ritchie et al., 2016; Le et al., 2017; Radev et al., 2020) offers a promising solution to the problem of repeated refits for models with or without tractable likelihood

functions. ABI decouples estimation into two phases: (1) a training phase, during which a neural network learns a posterior functional from model simulations, and (2) an inference phase, where posterior sampling is transformed into an almost instantaneous forward pass through the neural network. The term *amortized* emphasizes that the computational demand from the initial training phase amortizes over subsequent rapid model fits, typically within a fraction of a second when using invertible neural networks (Kruse et al., 2021). In the following, we describe posterior estimation with neural networks in more detail.

### 2.3.1 Neural posterior estimation

Neural posterior estimation (NPE) approximates the target posterior distribution  $p(\boldsymbol{\theta} | \mathbf{x})$  with a surrogate density  $q_\phi(\boldsymbol{\theta} | \mathbf{x})$ , where  $\phi$  denotes learnable weights of a generative neural network  $f_\phi$ . This so-called *inference network*  $f_\phi$  often implements a normalizing flow (Kobyzev et al., 2020) through a conditional invertible neural network (Ardizzone et al., 2019) capable of modeling complex target distributions. Such networks have demonstrated remarkable success in tackling amortized NPE problems across disciplines (e.g., Ardizzone et al., 2018; Gonçalves et al., 2020; Bieringer et al., 2021; von Krause et al., 2022; Avecilla et al., 2022). That said, other generative neural architectures, such as diffusion models (Sharrock et al., 2022), consistency models (Schmitt et al., 2024b), or flow matching (Wildberger et al., 2024) can be used for NPE as well and are fully compatible with our proposed methods. Below, we focus on normalizing flows (Kobyzev et al., 2020) as a concrete example of neural density estimation.

The normalizing flow represents an invertible learnable transformation between the intractable *target* (posterior) distribution and a tractable *base* distribution, such as a unit Gaussian. During training, the inference network minimizes the expected forward Kullback-Leibler (KL) divergence between the approximate posterior  $q_\phi(\boldsymbol{\theta} | \mathbf{x})$  and the true posterior  $p(\boldsymbol{\theta} | \mathbf{x})$  via backpropagation,

$$\begin{aligned} \hat{\phi} &= \arg \min_{\phi} \mathbb{E}_{(\boldsymbol{\theta}, \mathbf{x}) \sim p(\boldsymbol{\theta}, \mathbf{x})} \left[ \text{KL} \left( p(\boldsymbol{\theta} | \mathbf{x}) \parallel q_\phi(\boldsymbol{\theta} | \mathbf{x}) \right) \right] \\ &= \arg \min_{\phi} \mathbb{E}_{(\boldsymbol{\theta}, \mathbf{x}) \sim p(\boldsymbol{\theta}, \mathbf{x})} \left[ -\log q_\phi(\boldsymbol{\theta} | \mathbf{x}) \right] + \text{const}, \end{aligned} \quad (9)$$

where the expectation is approximated via its empirical mean over draws from the Bayesian model  $(\boldsymbol{\theta}, \mathbf{x}) \sim p(\boldsymbol{\theta}, \mathbf{x})$ . The density of the true posterior  $p(\boldsymbol{\theta} | \mathbf{x})$  is dropped from the objective in Equation 9 because it does not depend on the neural network parameters  $\phi$ . This procedure is self-consistent and recovers the *true posterior* under optimal convergence and a sufficiently expressive neural network (Ardizzone et al., 2019). Crucially for optimization and downstream inference tasks, we can evaluate the approximate posterior density  $q_\phi(\boldsymbol{\theta} | \mathbf{x})$  for any pair  $(\boldsymbol{\theta}, \mathbf{x})$  via the change-of-variables formula,

$$q_\phi(\boldsymbol{\theta} | \mathbf{x}) = p(\mathbf{z} = f_\phi(\boldsymbol{\theta}; \mathbf{x})) \left| \det \frac{\partial f_\phi(\boldsymbol{\theta}; \mathbf{x})}{\partial \boldsymbol{\theta}} \right|, \quad (10)$$

where  $f_\phi(\boldsymbol{\theta}; \mathbf{x})$  denotes a forward pass of parameters  $\boldsymbol{\theta}$  through the neural network  $f_\phi$ , conditional on data  $\mathbf{x}$ , and  $\mathbf{z}$  is a vector from the base distribution, typically  $\mathbf{z} \sim \text{Normal}(0, \mathbb{I})$ . Amortization is a direct consequence of the fact that we are using a single (global) set of neural network parameters  $\phi$  to approximate the posterior distribution for many data sets in the support of  $p(\boldsymbol{\theta}, \mathbf{x})$ . The structure of these data sets will vary in practice, for instance, with respect to their sample size  $N \in \mathbb{N}$ . This necessitates some form of preprocessing or compression before being passed to  $f_\phi$ , as discussed next.

### 2.3.2 Learned summary statistics

Directly using conditional invertible neural networks to learn the posterior distribution based on raw data has two main shortcomings: First, the data may be high-dimensional even though some (opaque) lower-dimensional representation would suffice to inform posterior inference. Second, these architectures cannot generally deal with data  $\mathbf{x} = \{\mathbf{x}_1, \dots, \mathbf{x}_N\}$  of varying lengths  $N$ , which is required to represent different sample sizes or time horizons.

To address both problems simultaneously, Radev et al. (2020) proposed to use a second neural network  $h_\psi$ , dubbed a *summary network*. The task of the summary network is to compress the data  $\mathbf{x}$  into a lower-dimensional representation  $h_\psi(\mathbf{x})$ , also known as summary statistics or embeddings. The network’s architecture depends on the structure of the data (e.g., permutation invariant network for exchangeable data, recurrent network for time-series data, etc.)<sup>1</sup>. Crucially, the summary network  $h_\psi$  and the inference network  $q_\phi$  are optimized in one joint *end-to-end* optimization objective,

$$\hat{\psi}, \hat{\phi} = \arg \min_{\psi, \phi} \mathbb{E}_{(\boldsymbol{\theta}, \mathbf{x}) \sim p(\boldsymbol{\theta}, \mathbf{x})} \left[ -\log q_\phi(\boldsymbol{\theta} | h_\psi(\mathbf{x})) \right], \quad (11)$$

<sup>1</sup>It is also possible to do away with *explicit summary statistics* (e.g., in transformer-based architectures, Gloeckler et al., 2024), but accessing these statistics can be beneficial in multiple ways, e.g., in detecting model misspecification (Schmitt et al., 2022) or robustifying inference (Huang et al., 2024).



such that the learned summary statistics are *approximately sufficient* (Chen et al., 2020; Radev et al., 2020) for posterior inference. As a consequence, the learned summary statistics  $h_\psi(\mathbf{x})$  are not generally sufficient to reconstruct the data set  $\mathbf{x}$  itself (i.e., as in traditional autoencoders). Instead, they merely approximate the Bayesian notion of sufficiency, where summary statistics are sufficient if they do not alter the posterior distribution when swapped with the data:  $p(\boldsymbol{\theta} | \mathbf{x}) = p(\boldsymbol{\theta} | h_\psi(\mathbf{x}))$ .

### 2.3.3 Sampling from the amortized neural estimator

Once optimization has been performed, the same pre-trained architecture can be applied to estimate the same model family on an unseen observed data set  $\mathbf{x}^{obs}$ . During inference, the pre-trained networks  $h_\psi$  and  $f_\phi$  are used to efficiently obtain draws from the approximate posterior  $q_\phi(\boldsymbol{\theta} | \mathbf{x}^{obs})$ . First, the summary network  $h_\psi$  compresses the observed data to a fixed-size vector  $h_\psi(\mathbf{x}^{obs})$ . Then, the invertible network  $f_\phi$  obtains  $S$  draws  $(\boldsymbol{\theta}^{(1)}, \dots, \boldsymbol{\theta}^{(S)})$  from the approximate posterior by sampling random multivariate unit Gaussian vectors  $(\mathbf{z}^{(1)}, \dots, \mathbf{z}^{(S)})$  and performing an *inverse pass* through the inference network, conditional on the summarized data  $h_\psi(\mathbf{x}^{obs})$ :

$$\boldsymbol{\theta}^{(s)} = f_\phi^{-1}(\mathbf{z}^{(s)}; h_\psi(\mathbf{x}^{obs})) \quad \text{with } \mathbf{z}^{(s)} \sim \text{Normal}(\mathbf{0}, \mathbb{I}) \quad \text{for } s = 1, \dots, S. \quad (12)$$

At this stage, no MCMC or importance sampling is performed, but multiple independent random draws from the posterior can efficiently be obtained *in parallel* because both sampling the latent vectors  $\mathbf{z}^{(s)}$  and the inverse pass through the neural network are readily parallelized. While the latent space typically follows a unit Gaussian distribution, other distributions like heavy-tailed Student- $t$  (Alexanderson and Henter, 2020) have been explored as well, which simply alters the sampling statement for  $\mathbf{z}^{(s)}$  in Equation 12.

### 2.3.4 Why are multilevel models challenging for neural posterior estimation?

As described above, using NPE with learned summary statistics has advantages over its non-amortized simulation-based counterparts (faster re-fits) or amortized likelihood-based algorithms (expressive neural architectures and allowing inference for models with implicit likelihoods). However, standard NPE is not well suited for estimating MLMs out of the box. This is due to MLMs' particular probabilistic symmetries that feature hierarchically layered stages in the generative forward model as well as multiple levels of exchangeability and interdependence that should be considered. In particular:

1. The number of groups and the number of observations within groups may vary (e.g., due to missingness), necessitating hierarchical summary networks aligned with the structure of the data.
2. The dimension of the joint posterior distribution depends on the number of groups and may also vary between data sets, necessitating hierarchical inference networks with varying numbers of outputs.
3. The dependencies between the two levels may vary (e.g., non-exchangeable observations, exchangeable groups), necessitating different types of summary and inference networks.

In what follows, we will present a neural architecture that is based on NPE with learned summary statistics and enables fully amortized Bayesian inference for MLMs with both tractable and intractable likelihoods. We call our method *Multi-Level Neural Posterior Estimation (ML-NPE)*.

## 2.4 Multilevel Neural Posterior Estimation

In an MLM with two levels and group indices  $j = 1, \dots, J$ , there are three qualitatively different kinds of parameters: (1) *Local parameters*  $\boldsymbol{\theta}_j$  that are specific for each group  $j$ , such as a separate intercepts or slopes per group; (2) *hyperparameters*  $\boldsymbol{\tau}$ , typically means and standard deviations for the local parameters as well as correlations among local parameters of the same group; and (3) *shared parameters*  $\boldsymbol{\sigma}$  with a direct effect on the likelihood function of all groups, without any hierarchical component. Building on the approach of Heinrich et al. (2023), we exploit the exchangeability of the groups by using two pairs of summary and inference networks: One network pair estimates the local parameters conditional on the group-level data and the global parameters, that is, the concatenation of hyper and shared parameters. The other network pair directly estimates the global parameters conditional on all available data.

To illustrate our ML-NPE method, consider a model with groups  $j = 1, \dots, J$  and  $N_j$  observations per group, where  $i = 1, \dots, N_j$  denotes the index of a given observational unit. Accordingly,  $\mathbf{x}_{j,i}$  is the (multivariate) observation of the  $i^{\text{th}}$  unit in the  $j^{\text{th}}$  group. As above, let  $\boldsymbol{\theta}_j$  be the set of local parameters in the  $j^{\text{th}}$  group,  $\boldsymbol{\tau}$  be hyperparameters, and  $\boldsymbol{\sigma}$  be shared parameters. Utilizing exchangeability of groups and observations within groups, the joint distribution

$p(\tau, \sigma, \theta_j, \mathbf{x}_{j,i})$  of all variables factorizes as:

$$p(\tau, \sigma, \{\theta_j\}, \{\mathbf{x}_{j,i}\}) = p(\tau) p(\sigma) \prod_{j=1}^J p(\theta_j | \tau) p(\mathbf{x}_j | \theta_j, \sigma) \quad (13)$$

The set notations  $\{\theta_j\}$  and  $\{\mathbf{x}_{j,i}\}$  highlight that both the number of groups and observations in each group can vary across simulations, datasets, or experiments. The goal of fully Bayesian inference is to obtain the *joint posterior distribution* of parameters conditioned on the observed data:

$$p(\tau, \sigma, \{\theta_j\} | \{\mathbf{x}_{j,i}\}) = \frac{p(\tau, \sigma, \{\theta_j\}, \{\mathbf{x}_{j,i}\})}{p(\{\mathbf{x}_{j,i}\})} \quad (14)$$

In a nutshell, our proposed method leverages the fact that the joint posterior can be further factorized into two parts, namely (1) the hyperparameters  $\tau$  together with the shared parameters  $\sigma$ ; and (2) the local parameters  $\theta_j$ :

$$\begin{aligned} p(\tau, \sigma, \{\theta_j\} | \{\mathbf{x}_{j,i}\}) &= p(\tau, \sigma | \{\mathbf{x}_{j,i}\}) p(\{\theta_j\} | \tau, \sigma, \{\mathbf{x}_j\}) \\ &= p(\tau, \sigma | \{\mathbf{x}_{j,i}\}) \prod_{j=1}^J p(\theta_j | \tau, \sigma, \mathbf{x}_j) \end{aligned} \quad (15)$$

In this way, we divide the problem of learning the full joint posterior into smaller problems of learning the joint posteriors at each level separately. To represent this posterior, we introduce two NPE sub-modules  $f_{\phi_1}(\tau, \sigma; h_{\psi_1}(\{\mathbf{x}_{j,i}\}))$  and  $f_{\phi_2}(\theta_j; h_{\psi_2}(\mathbf{x}_j), \tau, \sigma)$ , one for each of the two terms in Equation 15. The first inference network  $f_{\phi_1}$  learns a representation of the marginal distribution of hyper and shared parameters, while the second inference network  $f_{\phi_2}$  estimates the local parameters. When structured in this way, we can leverage the model-implied exchangeability of the local parameters  $\theta_j$  and employ weight sharing by only using a single network  $f_{\phi_2}$  for all local parameters  $\theta_j$ . Amortizing over the number of groups  $J$  greatly reduces the computational complexity because the total number of network parameters  $\phi = (\phi_1, \phi_2)$  is now independent of the number of groups  $J$ .

Similar to standard NPE with learned summary statistics, each inference network is also equipped with its respective summary network: The first summary network  $h_{\psi_1}$  learns a low-dimensional representation of the whole dataset  $\{\mathbf{x}_{j,i}\}$ , while the second summary network  $h_{\psi_2}$  only requires observations of the specific group  $j$  alongside its global and shared parameters which are processed by the second inference network  $f_{\phi_2}$ . This is possible because the local parameters  $\theta_j$  for each group are conditionally independent of the data in other groups, given the hyper and shared parameters.

Writing  $\phi = (\phi_1, \phi_2)$  for the weights of the inference networks and  $\psi = (\psi_1, \psi_2)$  for the weights of the summary networks, our optimization criterion from Equation 11 becomes

$$\hat{\psi}, \hat{\phi} = \arg \min_{\psi, \phi} \mathbb{E}_{(\tau, \sigma, \theta, \mathbf{x}) \sim p(\tau, \sigma, \theta, \mathbf{x})} \left[ -\log q_{\phi}(\tau, \sigma, \{\theta_j\} | \{\mathbf{x}_{j,i}\}) \right], \quad (16)$$

where we denote exchangeable replications with a subscript. The negative log-density term inside the expectation can now be decomposed into:

$$\begin{aligned} -\log q_{\phi}(\tau, \sigma, \{\theta_j\} | \{\mathbf{x}_{j,i}\}) &= -\log q_{\phi_1}(\tau, \sigma | h_{\psi_1}(\{\mathbf{x}_{j,i}\})) \\ &\quad - \sum_{j=1}^J \log q_{\phi_2}(\theta_j | h_{\psi_2}(\mathbf{x}_j), \tau, \sigma), \end{aligned} \quad (17)$$

which can be optimized in closed-form via backpropagation.

## 2.5 Amortized sampling from ML-NPE

Once training has converged, the networks can be stored and applied multiple times to arbitrary numbers of observations (data sets) of the form  $\{\mathbf{x}_{j,i}\}$ . For each data set, we can obtain draws from the joint posterior via inverse ancestral sampling by applying the transformation of each conditional invertible neural network module to random draws from the corresponding base distributions:

$$\begin{aligned} (\tau^{(s)}, \sigma^{(s)}) &\sim q_{\phi_1}(\tau, \sigma | h_{\psi_1}(\{\mathbf{x}_{j,i}\})) \\ \theta_j^{(s)} &\sim q_{\phi_2}(\theta_j | h_{\psi_2}(\tau^{(s)}, \sigma^{(s)}, \mathbf{x}_j)) \end{aligned} \quad (18)$$

This makes sampling at each level very efficient since only single passes through the pre-trained invertible modules are required. Second, no draws are rejected or thinned (as in MCMC methods), since, assuming perfect convergence, the networks generate independent samples from the true joint posterior (Ardizzone et al., 2019). In practice, perfect convergence can rarely be achieved, so some approximation error is to be expected. Fortunately, we can diagnose approximation errors either directly by inspecting the base distributions over different simulated data sets or indirectly, by performing inferential calibration checks (see Section 3 for more details). Third, due to the application of specialized summary networks as conditioners, the networks do not need to be re-trained for different individual sample sizes or groups. This implies that different types of cross-validation can also be efficiently implemented by re-using the same pre-trained architecture. Finally, since we approximate the expectation in Equation 17 via its empirical mean over simulations from the generative model, we require no closed-form likelihood function or potential numerical integration of a complex likelihood, which makes ML-NPE applicable to intractable models.

## 2.6 Alternative factorizations

The factorization in Equation 15 is not unique. An equally valid factorization would be:

$$p(\tau, \sigma, \{\theta_j\} | \{x_{j,i}\}) = p(\tau | \{\theta_j\}) p(\sigma | \{x_{j,i}\}, \{\theta_j\}) p(\{\theta_j\} | \{x_{j,i}\}), \quad (19)$$

which suggests a different neural inference architecture consisting of three components  $f_{\phi_1}(\tau; h_{\psi_1}(\{\theta_j\}))$ ,  $f_{\phi_2}(\sigma; h_{\psi_{21}}(\{x_{j,i}\}), h_{\psi_{22}}(\{\theta_j\}))$ , and  $f_{\phi_3}(\{\theta_j\}; h_{\psi_3}(\{x_{j,i}\}))$ . For this factorization, we utilize the fact that the global parameters  $\tau$  are completely identified by the local parameters  $\theta_j$ . We now also require an additional inference network solely for the shared parameters  $\sigma$ , as they are not identified by the local parameters alone. Compared to the factorization in Equation 15, this architecture cannot easily be amortized over the number of groups, because we lack a per-group summary and inference networks.

We could improve this architecture by introducing the following modifications. First, we split the single summary network  $h_{\psi_3}$  in the sub-module for the local parameters into two summary networks:  $h_{\psi_{31}}(\{x_{j,i}\})$  learns a representation of the global data structure (i.e., sufficient statistics to determine the degree of required shrinkage) and  $h_{\psi_4}(x_j)$  learns a representation of the local data structure of group  $j$ . Second, we redefine  $f_{\phi_3}$  into a per-group inference network  $f_{\phi_3}(\theta_j; h_{\psi_{31}}(\{x_{j,i}\}), h_{\psi_{32}}(x_j))$  to be applied  $J$  times, once for each group. This restores amortization capabilities and keeps the output dimensionality of all inference networks constant regardless of the dataset. However, the implied architecture is more involved, requiring up to 5 summary and 3 inference networks, instead of only 2 summary and 2 inference networks for the factorization presented in Equation 15. For this reason, we decided to further study only the latter, structurally simpler architecture in our empirical evaluations.

## 3 Empirical evaluation

We evaluate our two-level neural architecture in 3 different applications based on real-world data sets that aim to cover a broad spectrum of use cases for multilevel models in practice. Concretely, the applications encompass 1) an autoregressive time-series model that predicts air passenger traffic between different European countries and the US, 2) a drift-diffusion model to infer latent parameters of a decision-making process from reaction time data, 3) a model to infer style parameters of handwriting from high-dimensional image data. All experiments are implemented with the BayesFlow software for amortized Bayesian workflows with neural networks (Radev et al., 2023b).

**Evaluation metrics** For each application, we implement a series of model checks: We perform simulation-based calibration (SBC) to ensure that our neural posterior estimation algorithm samples from the correct posterior. Given a perfect approximation of the true posterior  $p(\theta | x)$ , for any quantile  $q \in (0, 1)$ , a  $q \times 100\%$  posterior interval contains the true value in approximately  $q \times 100\%$  of the cases. SBC flags violations of posterior calibration which hints at issues with computational validity, for example arising from insufficient simulation-based training or a lack of expressiveness of the neural networks.

To detect model misspecification, we perform posterior predictive checks. We investigate inferential accuracy by providing graphical comparisons of posterior intervals and ground truth parameter values over the test set. When computationally feasible, we also fit each model in Stan and provide plots of posterior intervals to compare the estimates against a known to be reliable reference algorithm. For the last model check, we explicitly compare shrinkage of the group-level parameters between our neural framework and Stan, as we expect that any subtle algorithmic error would likely first manifest as incorrect posterior shrinkage.



### 3.1 Experiment 1: Air passenger traffic

We apply our neural architecture to analyze trends in European air passenger traffic data provided by Eurostat (2022a,b,c). Using this case study, we highlight that our neural architecture can correctly and efficiently amortize over both the number of groups and the number of observations per group, as well as over spaces of covariates. By using a summary network that is aligned to the structure of data, we also show that our approach can be easily extended to estimate non-IID response variables. We provide a systematic calibration and shrinkage analysis to verify correct inference at each hierarchy level.

**Model description** We obtained time series of annual air passenger counts between 16 European countries (departures) and the United States of America (destination) from 2004 to 2019 and fit the following autoregressive multilevel model:

$$y_{j,t+1} \sim \text{Normal}(\alpha_j + y_{j,t}\beta_j + u_{j,t}\gamma_j + w_{j,t}\delta_j, \sigma_j), \quad (20)$$

where the target quantity  $y_{j,t+1}$  is the difference in air passenger traffic for country  $j$  between time  $t + 1$  and  $t$ . To predict  $y_{j,t+1}$ , we use two additional predictors: The first predictor  $u_{j,t}$  is the annual household debt of country  $j$  at time  $t$ , measured in % of gross domestic product (GDP), and the second predictor  $w_{j,t}$  is the real GDP per capita. The parameters  $\alpha_j$  are the country-level intercepts,  $\beta_j$  are the autoregressive coefficients,  $\gamma_j$  are the regression coefficients of the household debt predictor,  $\delta_j$  are the regression coefficients for the GDP per capita predictor,  $\sigma_j$  is the standard deviation of the noise term,  $\mu$  are the hierarchical means for local parameters,  $\sigma$  are the hierarchical standard deviations for the local parameters, Normal is the normal distribution parameterized by mean and standard deviation and Normal<sup>+</sup> is the corresponding half-normal distribution (truncated at zero).

Mapping the notation in this applied modeling task to the taxonomy of previous sections, the observables  $\mathbf{x}$  are now split into a target  $y$  and predictors  $(u, w)$  with group-structure defined by the country index  $j$ . We use the following prior distribution:

$$\begin{array}{lll} \alpha_j \sim \text{Normal}(\mu_\alpha, \sigma_\alpha) & \mu_\alpha \sim \text{Normal}(0, 0.5) & \sigma_\alpha \sim \text{Normal}^+(0, 0.25) \\ \beta_j \sim \text{Normal}(\mu_\beta, \sigma_\beta) & \mu_\beta \sim \text{Normal}(0, 0.2) & \sigma_\beta \sim \text{Normal}^+(0, 0.15) \\ \gamma_j \sim \text{Normal}(\mu_\gamma, \sigma_\gamma) & \mu_\gamma \sim \text{Normal}(0, 0.5) & \sigma_\gamma \sim \text{Normal}^+(0, 0.25) \\ \delta_j \sim \text{Normal}(\mu_\delta, \sigma_\delta) & \mu_\delta \sim \text{Normal}(0, 0.5) & \sigma_\delta \sim \text{Normal}^+(0, 0.25) \\ \log(\sigma_j) \sim \text{Normal}(\mu_\sigma, \sigma_\sigma) & \mu_\sigma \sim \text{Normal}(-1, 0.5) & \sigma_\sigma \sim \text{Normal}^+(0, 1) \end{array} \quad (21)$$

As commonly done for autoregressive models, we regress on the differences between time periods to reduce issues due to non-stationarity. This is particularly important in an SBI setting, because for  $\beta_j > 1$  the time series would exhibit strong exponential growth that would quickly surpass reasonable air traffic volumes, creating highly unrealistic simulations.

**Model training** To generate training data for the neural approximator, we utilize an ancestral sampling scheme: First, a sample is drawn from the distribution of hyperparameters  $p(\boldsymbol{\tau})$ . We then draw  $M$  samples from the conditional distribution of group-level parameters  $p(\alpha_j, \beta_j, \gamma_j, \sigma_j \mid \boldsymbol{\tau})$ , where  $\boldsymbol{\tau}$  denote the hyperparameters and each of the  $M$  draws corresponds to a country. For each country, we then simulate a time series from the conditional likelihood  $p(y_{j,t+1} \mid \alpha_j, \beta_j, \gamma_j, \sigma_j, \mathbf{u}_j, \mathbf{w}_j)$ . We amortize over the number of countries  $M$  as well as the number of observed time points  $T$ . The neural approximator is therefore able to generate draws from the posterior  $p(\boldsymbol{\tau}, \alpha_j, \beta_j, \gamma_j, \sigma_j \mid \mathbf{y}_j, \mathbf{u}_j, \mathbf{w}_j)$  for data sets with a varying number of countries as well as a varying number of time points without any further training. To facilitate training on simulated data and without loss of generality, we assume that each time series starts at  $y_{j,t=1} \sim \text{Normal}(0.5, 1)$ .

The network architecture for amortized posterior inference consists of a local summary network with an initial long short-term memory (LSTM; Hochreiter and Schmidhuber, 1997) layer capturing time dependencies of these input data, followed by a dense layer with 256 units and exponential linear unit activation function and another dense layer with 32 units. For the global summary network, we use a set transformer (Lee et al., 2018) with 32 summary dimensions, 16 inducing points and 2 hidden layers with 64 units with a rectified linear unit (ReLU; Agarap, 2018) activation function. The multihead attention layer of the set transformer uses an attention block with 4 heads and key dimension 32 with 1% dropout. For the inference networks, we use neural spline flows (Durkan et al., 2019) with 6 coupling layers using 2 dense layers with 256 units each, a ReLU activation function and 5% dropout. We set the simulation budget to  $N = 100000$  and train for 200 epochs using the Adam (Kingma and Ba, 2014) optimizer with an initial learning rate of  $5 \times 10^{-4}$  with cosine decay (Loshchilov and Hutter, 2016) and a batch size of 32.

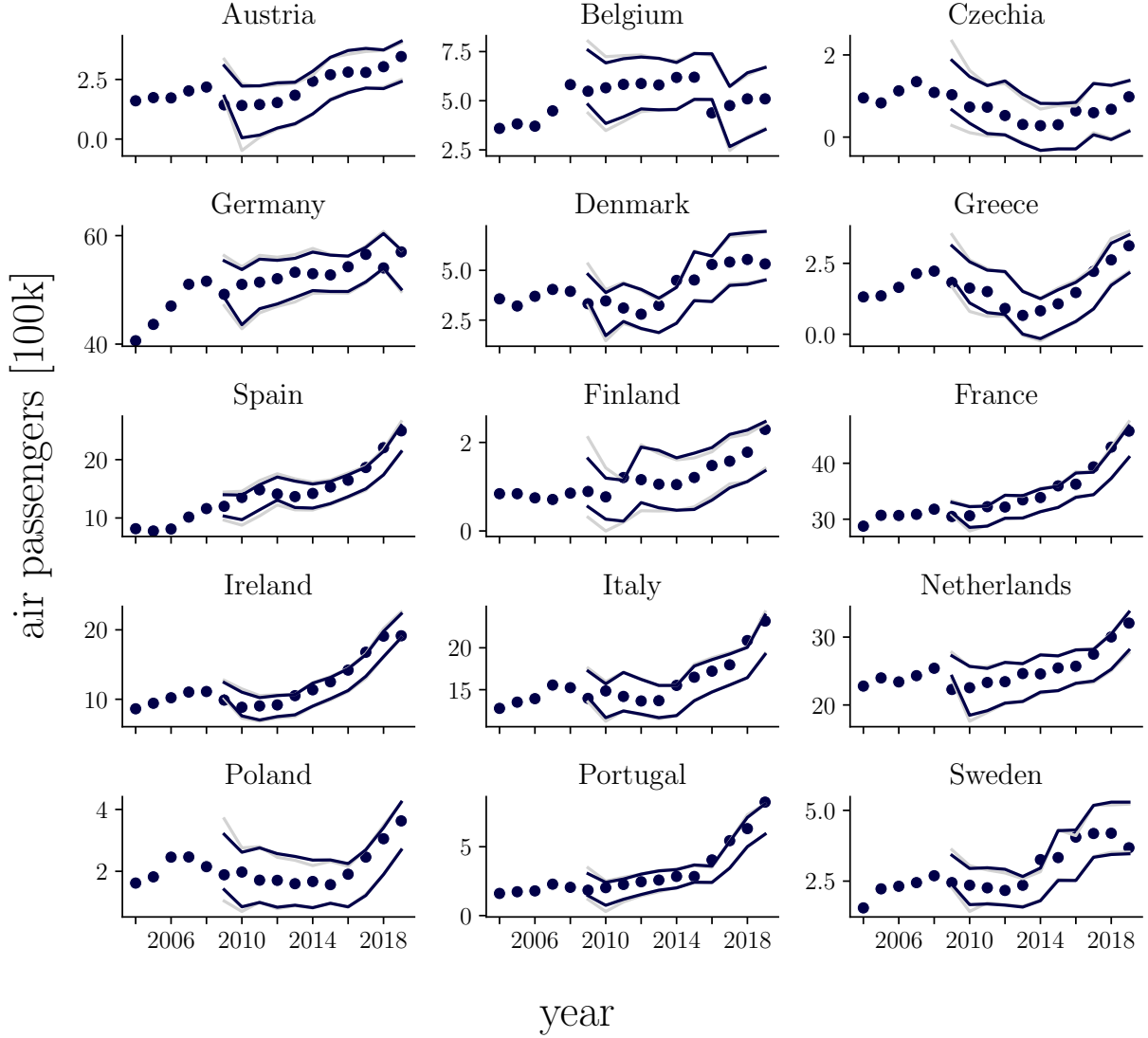


Figure 1: Annual air passenger traffic volume in 100 thousand passengers between different European countries and the United States of America. Blue points show observed data, blue lines show 95% uncertainty intervals of the 1-step ahead posterior predictive distribution. For reference, grey lines show draws from the posterior predictive distribution of the same model fitted in Stan. The posterior predictive checks show that the model predictions are consistent with the observed data and draws from the posterior predictive distribution obtained by the reference implementation in Stan are indistinguishable from draws obtained by our amortized ML-NPE method.

**Posterior predictive checks** To ensure that the simple AR(1) model is adequate enough to describe the observe data, [Figure 1](#) shows the observed time series overlaid with draws from the posterior predictive distribution obtained by our ML-NPE method as well as a reference implementation in Stan. While predictive uncertainty is high, presumably in part because of the relatively simple model, short time series and predictors that only weakly associated with the response variable, the predictions from the AR(1) model are consistent with the observed data.

**Posterior inference** [Figure 2](#) and [Figure 3](#) shows posterior recovery and calibration on 100 simulated validation datasets. We observe good posterior recovery and calibration for all parameters.

To validate that we also observe good posterior recovery on real data, we perform posterior inference on the [Eurostat \(2022a,b,c\)](#) dataset and contrast the results to the posterior intervals obtained by the Stan reference implementation (see

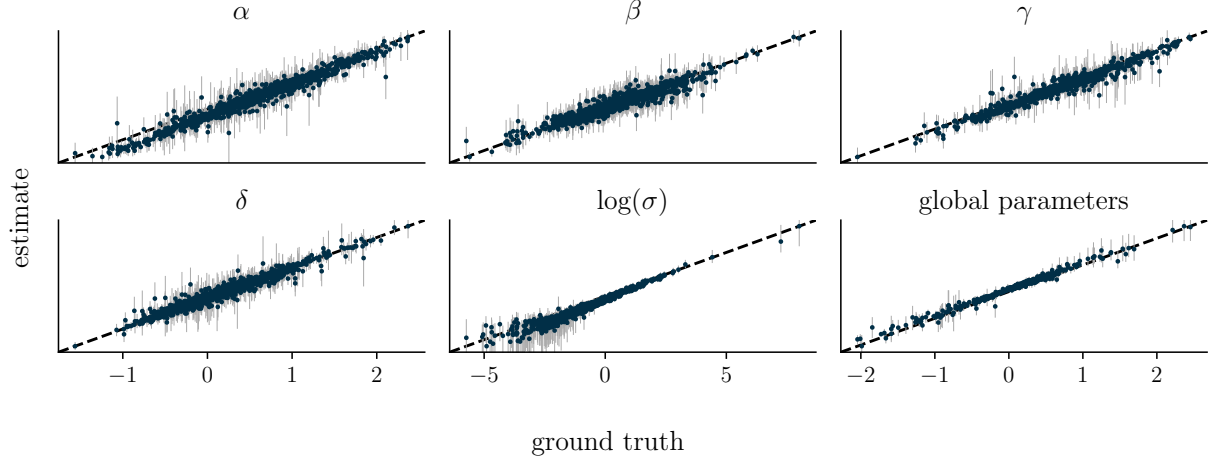


Figure 2: Posterior recovery on 50 simulated validation datasets. All parameters show good posterior recovery and calibration, indicating that our ML-NPE is able to recover true parameter values without bias and accurate uncertainty quantification.

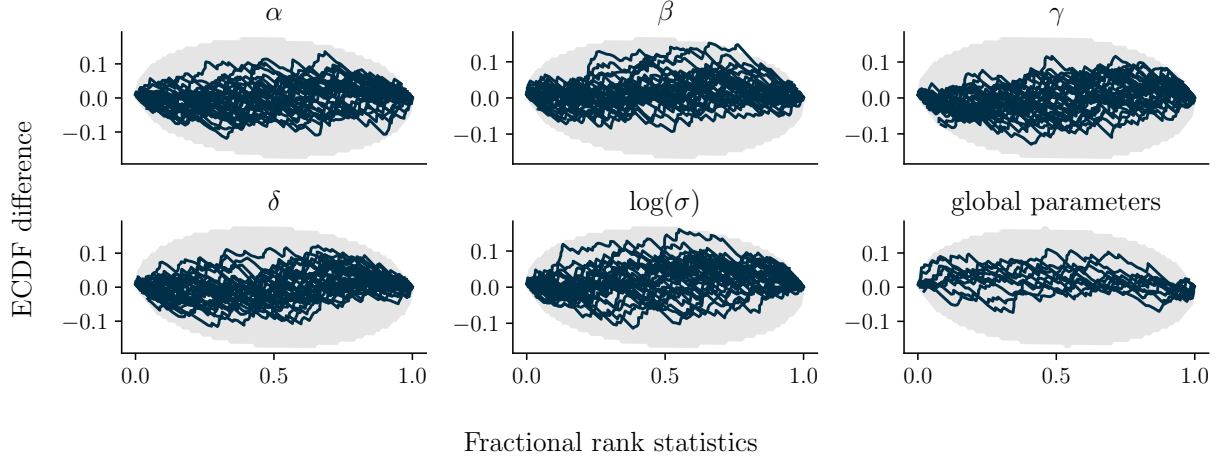


Figure 3: Simulation-based calibration plots. ECDF difference is the difference between the empirical cumulative distribution function of the rank distribution (obtained by comparing the rank of prior draws with their corresponding posterior draws) and the uniform cumulative distribution function. For the parameters  $\alpha$ ,  $\beta$ ,  $\gamma$ ,  $\delta$ , and  $\log(\sigma)$ , each line represents a group-level parameter (i.e., the country-specific estimate). The panel *global parameters* contains the estimated mean and standard deviation for each of the 5 group-level parameters. All lines lie within the shaded 99% simultaneous confidence bands, indicating well-calibrated marginal posterior distributions.

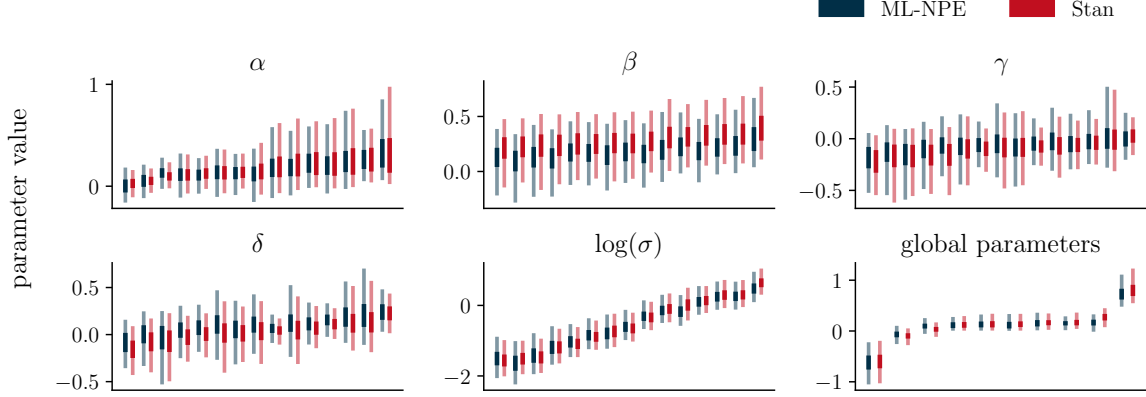


Figure 4: Posterior intervals obtained from amortized ML-NPE (ours) and the gold-standard HMC reference, as implemented via Stan. Plots show the central 50% (dark) and 95% (light) posterior credible intervals based on quantiles. For the parameters  $\alpha$ ,  $\beta$ ,  $\gamma$ ,  $\delta$ , and  $\log(\sigma)$ , each interval pair refers to a single group-level parameter (one for each country). For the global parameters, each interval pair refers to a hyperparameter (one mean and one standard deviation for each of the group-level parameters, so 10 hyperparameters in total). The parameters are sorted by increasing mean (as per Stan) to ease interpretation of shrinkage towards a common mean.

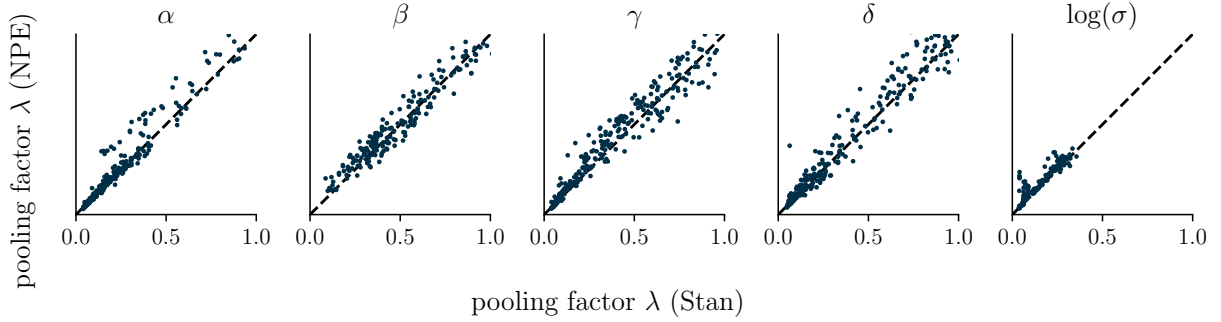


Figure 5: Posterior shrinkage observed in 100 simulated datasets via our ML-NPE methods to the results obtained by Stan. The scatter points lie along the diagonal, indicating that our method is able to correctly shrink group-level regression coefficients towards their common mean.

Figure 4). Model tests on non-simulated data are particularly important in amortized Bayesian inference because of a possible amortization gap: If the simulated data used for training does not lie within the scope of data the model is going to be applied on, ABI might yield posterior draws that are far off from the true posterior. The plot shows that the results obtained by ML-NPE are consistent with the results obtained by Stan.

**Posterior shrinkage** To identify if our approach partially pools the local parameters correctly towards their common mean, we compare posterior shrinkage of our ML-NPE method to a reference implementation in Stan. We quantify posterior shrinkage via the pooling factor, which describes how much the group-level coefficients are shrunk towards the common mean. Following Gelman and Hill (2006), the pooling factor  $\lambda_j$  for a local parameter  $\theta_j$  is calculated as  $\lambda_j = \frac{\text{sd}(\theta_j - \mu_\theta)^2}{\sigma_\theta^2}$ , where  $\mu_\theta$  and  $\sigma_\theta$  are the hierarchical mean and hierarchical standard deviation for a local parameter  $\theta_j$ . A pooling factor of  $\lambda_j = 0$  denotes no shrinkage and a posterior estimate that is identical to the no-pooling solution, whereas a shrinkage coefficient of  $\lambda_j = 1$  denotes complete shrinkage towards the hierarchical mean.

Figure 5 shows scatter plots of pooling factors for each parameter obtained on 100 simulated datasets via our ML-NPE method compared to pooling factors obtained on the same data via Stan. The scatter points lie along the diagonal, indicating correct shrinkage behavior of our ML-NPE method.

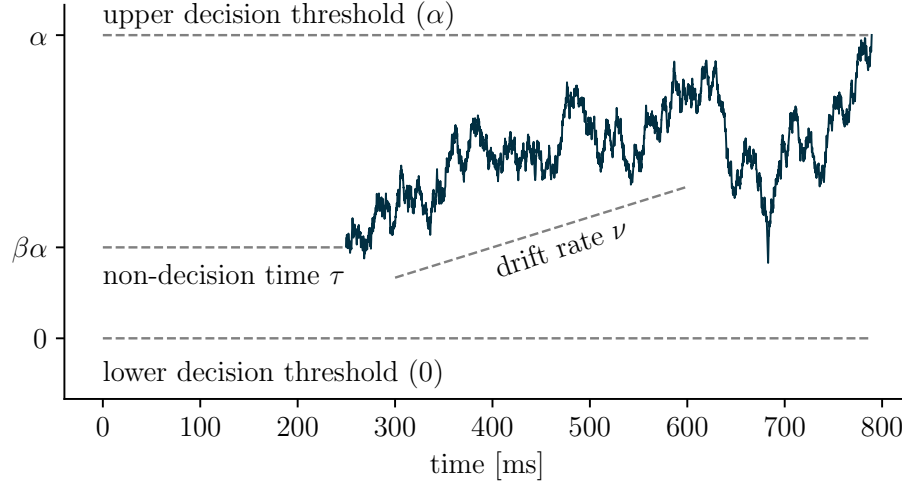


Figure 6: Example of a latent evidence trajectory for a single subject. The decision making process is modeled as a random walk that is governed by 4 parameters: The non-decision time  $\tau$  is the time until evidence accumulation begins and captures components that are not directly related to the decision, such as time spent on processing of sensory information. The drift rate  $\nu$  corresponds to the rate of information uptake. The decision threshold  $\alpha$  can be interpreted as the amount of evidence necessary to make a decision and is thus a measurement of response caution. The starting point  $\beta$  quantifies a subject’s tendency to prefer one choice over the other.

### 3.2 Experiment 2: Diffusion Decision Model

To test if ML-NPE is able to estimate a broad range of hierarchical structures and can achieve good calibration, we apply our method to a common decision-making model in psychology, neuroscience, and the cognitive sciences. We also use this case study to highlight key advantages of amortized Bayesian inference compared to posterior inference based on Hamiltonian Monte Carlo by performing near-instantaneous leave-one-group-out (LOGO) cross-validation. Additionally, we show that ML-NPE can reliably amortize over both the number of groups and observations, enabling fast and reliable posterior inference for almost arbitrary datasets in this model class.

**Model description** Consider a simple decision task, for example a setting where participants are presented with sequences of letters and asked to differentiate between words and non-words (i.e., a lexical decision task). The Diffusion Decision Model (DDM; Ratcliff et al., 2016) simultaneously models this binary decision and the response time via a continuous evidence-accumulation process: After an initial non-decision time, evidence accumulates following a noisy diffusion process with a certain drift rate until one of the two decision thresholds corresponding to the two choices is hit. For each subject, the latent evidence trajectory is governed by 4 parameters: A non-decision time  $\tau$ , a drift rate  $\nu$ , a decision threshold  $\alpha$ , and a bias (starting point)  $\beta$  (see Figure 6).

The nested structure of individual observations within subjects lends itself to a multilevel model where subject-specific estimates share information via common hyper-priors. For the first part of this case study, we consider subject-specific estimates for the non-decision time  $\tau$ , drift rate  $\nu$  and decision threshold  $\alpha$  (local parameters), while estimating a global bias  $\beta$  for all subjects (shared parameter). The generative model is summarized as:

$$\begin{aligned}
 \mu_\nu &\sim \text{Normal}(0.5, 0.3) & \mu_\alpha &\sim \text{Normal}(0, 0.05) & \mu_\tau &\sim \text{Normal}(-1, 0.3) \\
 \log \sigma_\nu &\sim \text{Normal}(-1, 1) & \log \sigma_\alpha &\sim \text{Normal}(-3, 1) & \log \sigma_\tau &\sim \text{Normal}(-1, 0.3) \\
 \nu_j &\sim \text{Normal}(\mu_\nu, \sigma_\nu) & \log \alpha_j &\sim \text{Normal}(\mu_\alpha, \sigma_\alpha) & \log \tau_j &\sim \text{Normal}(\mu_\tau, \sigma_\tau) \\
 \beta &\sim \text{Beta}(50, 50) \\
 \mathbf{y}_j &\sim \text{DDM}(\nu_j, \alpha_j, \tau_j, \beta),
 \end{aligned} \tag{22}$$

where  $\mathbf{y}_j$  is the vector containing tuples of decisions and reaction times for subject  $j$ , DDM is the likelihood of the 4-parameter diffusion decision model,  $\beta$  is the shared bias for all subjects, Beta is the Beta distribution with shape



parameters  $a$  and  $b$ , Normal is the normal distribution with mean  $\mu$  and standard deviation  $\sigma$ , and  $\nu_j, \alpha_j, \tau_j$  are the subject-specific drift rate, boundary threshold and non-decision time parameters, respectively. The priors were chosen based on prior predictive checks to match the range of typical outcomes for such decision tasks.

**Model training** We use the following network architecture for posterior inference: The local summary network consists of a set transformer with 16 summary dimensions, 32 inducing points, 2 hidden layers with 64 units with a rectified linear unit (ReLU) activation function and Glorot uniform initializer (Glorot and Bengio, 2010). The multihead attention layer utilizes an attention block with 4 heads and key dimension 32 with 1% dropout. The architecture of the global summary network is identical to that of the local summary network, except using 16 inducing points and 32 summary dimensions. For the inference networks, we use neural spline flows with 4 hidden layers for both local and global approximators.

To generate data for network training, we use the same ancestral sample scheme as for the air traffic case study in Subsection 3.1: First, we generate  $N$  random draws from the hyper-priors. For each of these  $N$  random draws, we then draw  $N_{\text{groups}}$  draws from the corresponding subject specific, local parameters. For each subject, we simulate  $N_{\text{obs}}$  observations from the diffusion process. To facilitate amortization over different group and observation sizes, we randomly draw values of  $N_{\text{obs}}$  from a uniform distribution with lower and upper bounds of 1 and 100 and draw  $N_{\text{obs}}$  from a uniform distribution with lower and upper bounds of 10 and 30. We set the initial simulation budget to  $N = 10000$  and train for 200 epochs using the Adam optimizer with an initial learning rate of  $5 \times 10^{-4}$  and a batch size of 32.

**Posterior inference** Figure 7 shows posterior recovery and calibration on 100 simulated validation datasets. We observe good posterior recovery and calibration for all parameters. However, calibration for the non-decision time  $\tau$  is not perfect, which is likely a result of the strong posterior contraction, as  $\tau$  shows good posterior recovery.

To validate that we also observe accurate posterior inference on non-simulated data, we contrast these results to model fits on experimental data published by Wagenmakers et al. (2008). In total, 17 subjects were asked to make 32 word/non-word decisions in each of the 20 trial blocks. The experiment was repeated in two conditions: Once after asking the subjects to focus on accuracy and once after asking the subjects to focus on speed. Figure 8 shows marginal posterior densities for the model fit on a subset of the data (observations in the accuracy condition in trial block 4) compared to the results obtained by Stan as a gold standard for reliable posterior inference. The results obtained by ML-NPE closely match the results obtained by Stan. We only use a subset of the data to better align with the model structure outlined in Section 3.2, our proposed ML-NPE algorithm can also be easily adapted to account for different trial conditions and block designs.

**Leave-one-group-out cross-validation** Amortized Bayesian inference is not only useful when performing posterior inference on many different data sets. Refitting the model multiple times on different subsets of the data is also required for many essential steps in the modern Bayesian workflow (Gelman et al., 2020) like cross-validation (Vehtari et al., 2017; Merkle et al., 2019) and simulation-based calibration (Talts et al., 2018). For multilevel models, it is often of practical interest to estimate and compare the predictive performance of models on new groups, leading to leave-one-group-out (LOGO) cross-validation. As the LOGO posterior is often vastly different from the full posterior because the local parameters for the left out group are only identified via their hyperparameters, approximation methods like Pareto-smoothed importance sampling (Vehtari et al., 2024) almost always fail. Performing LOGO cross-validation then requires refitting the model once for each group in the dataset, quickly rendering model comparison computationally infeasible when relying on, for example, MCMC algorithms for posterior inference. With amortized posterior inference, obtaining the LOGO posterior is almost instant (fraction of a second for our architectures), as it does not require refitting the model for each data subset.

To show that our ML-NPE method enables model comparison for multilevel models that are otherwise computationally infeasible, we contrast the previously described diffusion decision model in Section 3.2 with another model variant that also estimates  $\beta$  hierarchically. Instead of a single shared  $\beta$  for all subjects, this model variant estimates subject-specific  $\beta_j$  that share common hyper-priors. We make the following adjustments compared to the previous description of the drift diffusion model:

$$\beta_j \sim \text{BetaProportion}(\mu_\beta, \kappa_\beta) \quad \mu_\beta \sim \text{Beta}(50, 50) \quad \kappa \sim \text{Gamma}(5, 3), \quad (23)$$

where  $\beta_j$  is the bias for subject  $j$ , BetaProportion is the Beta distribution parameterized by a mean  $\mu_\beta$  and concentration parameter  $\kappa_\beta$ . The Beta proportion distribution is linked to the (standard) shape parameterization of the Beta distribution via the relation  $\alpha = \mu\kappa$  and  $\beta = (1 - \mu)\kappa$ . This adapted version of the diffusion decision model also illustrates that ML-NPE can estimate non-normal hyper-prior distributions.

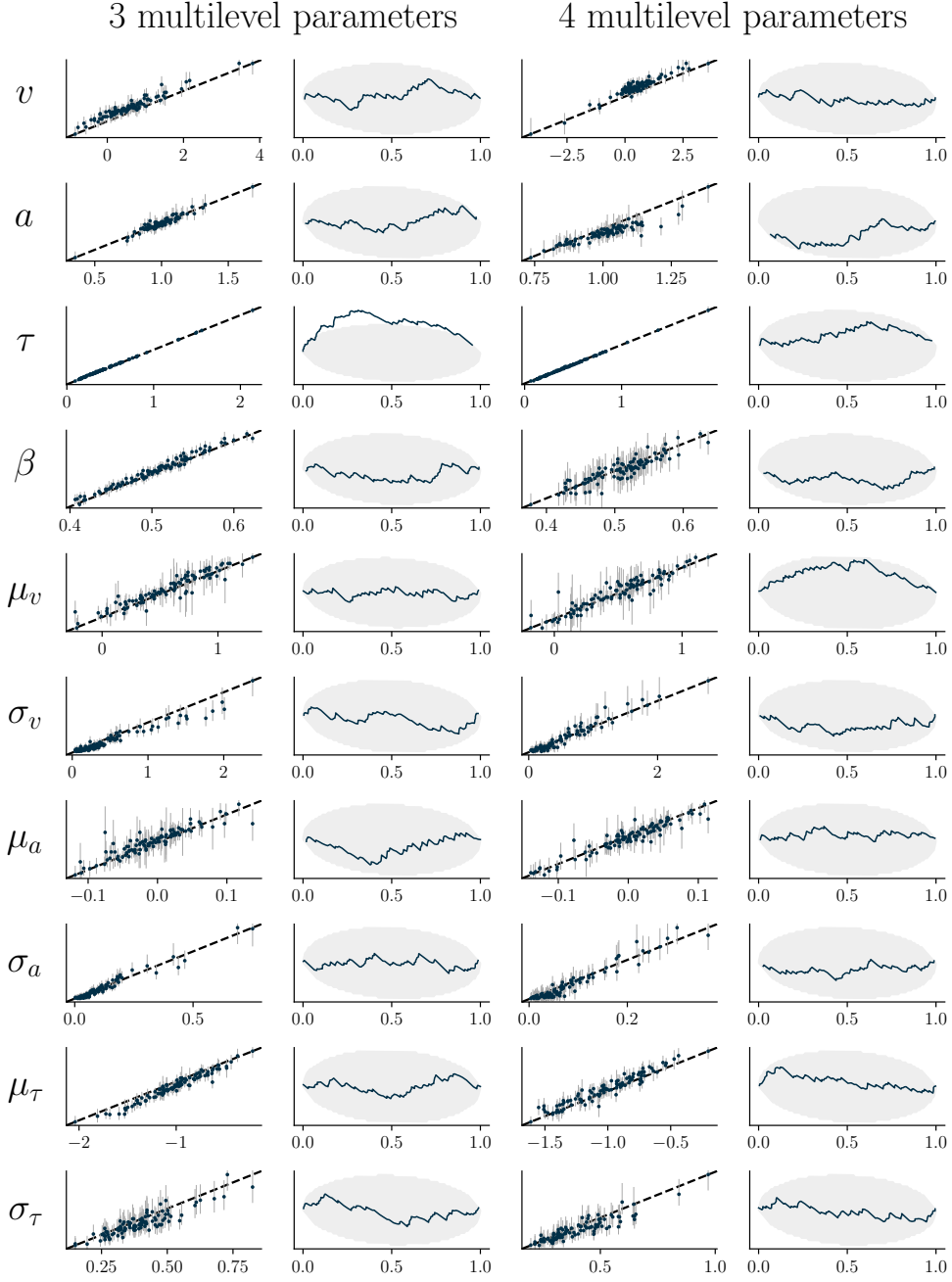


Figure 7: Posterior recovery (columns 1 and 3) and calibration (columns 2 and 4) for the diffusion decision model on 100 simulated validation datasets. The first two columns correspond to a model where a single  $\beta$  is estimated for all subjects (shared parameter). The last two columns correspond to a model where  $\beta$  is also estimated hierarchically (see the text for details). All parameters show good posterior recovery and calibration, except  $\tau$  in the model with 3 hierarchical parameters. As we observe particularly strong posterior contraction for this parameter, even minor deviations in posterior coverage would be detected as miscalibration. Therefore, the observed miscalibration for  $\tau$  is unlikely to have any meaningful impact in practical settings.

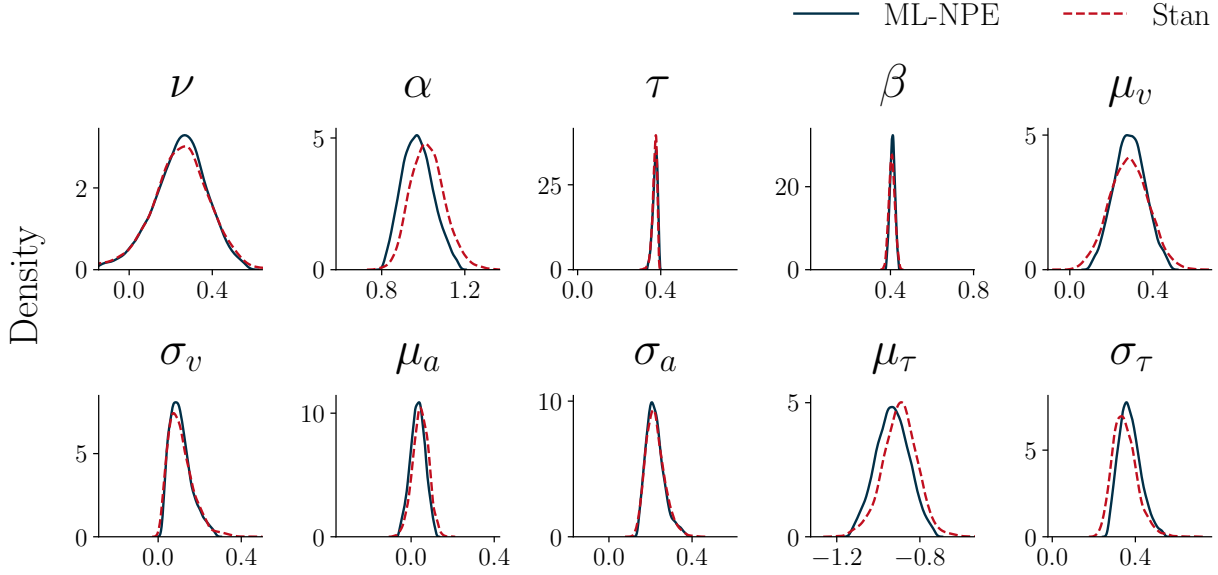


Figure 8: Marginal posterior distributions of the drift diffusion model fitted on experimental data. Blue kernel density plots were obtained by our ML-NPE method, red dashed lines show the results obtained by Stan as a gold standard for reliable posterior inference. The plots show that marginal posteriors obtained by ML-NPE are highly similar to the marginal posteriors obtained by Stan.

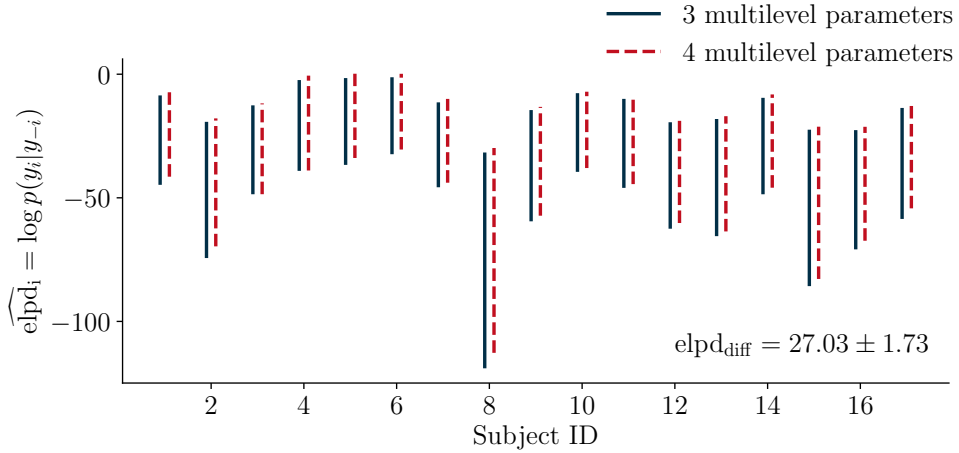


Figure 9: LOGO cross-validation on trial block 4 of the experimental dataset published by [Wagenmakers et al. \(2008\)](#). Vertical lines show central 80% posterior intervals based on quantiles. LOGO cross-validation is performed by leaving out each of the 17 subjects, refitting the model and quantifying predictive performance via ELPD. The blue vertical bars correspond to the model variant with 3 local parameters ( $\nu_j$ ,  $\alpha_j$ ,  $\tau_j$ ) and a shared  $\beta$  for all subjects, the red dashed lines correspond to a more flexible model that estimates all 4 parameters ( $\nu_j$ ,  $\alpha_j$ ,  $\tau_j$ ,  $\beta_j$ ) as local. The computed ELPD difference indicates a substantially better fit of the more flexible model with 4 local parameters per subject.

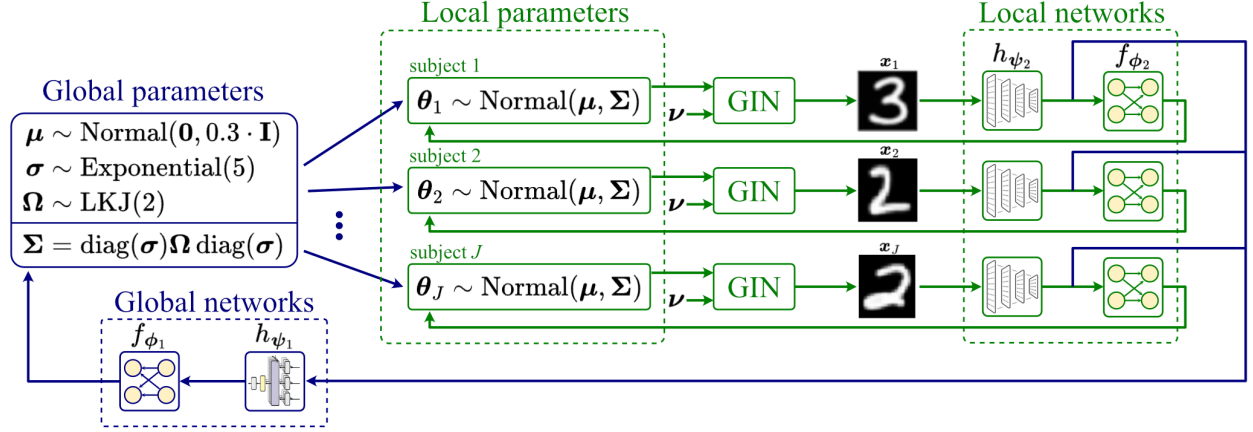


Figure 10: **Experiment 3.** Overview of the hierarchical model of digit style inference.

Figure 9 shows expected log predictive density (ELPD; Vehtari et al., 2017) values for each subject obtained by first removing subject  $j$  from the dataset, generating samples from the LOGO posterior and then evaluating the predictive performance on the left-out subject. The ELPD difference between the models with vs. without subject-specific  $\beta_j$  evaluates to  $\text{ELPD}_{\text{diff}} \approx 27.03$ , which is several times larger than its standard error  $\text{SE}_{\text{diff}} \approx 1.73$ . That is, there is strong statistical evidence that the model with varying  $\beta_j$  has better predictive performance on data of a previously unseen group.

Performing such a model comparison is computationally efficient in an amortized Bayesian inference setting, but quickly becomes infeasible when the model is fit using MCMC-based algorithms. In this example, using Stan to draw 1000 samples (after 1000 warm-up draws) from 4 chains in parallel takes about 6 minutes on a standard desktop processor, resulting in a total runtime of about 1.5 hours for all subjects. In contrast, training the amortized model using ML-NPE takes about 1 hour on a standard desktop graphics card, subsequently allowing almost instant inference (fraction of a second) of the LOGO posteriors. This comparison demonstrates that the required training time of amortized methods can quickly pay off, even in scenarios where one is only interested in evaluating a single dataset on which cross-validation is performed. This is particularly true if the number of groups is large, with growing gains for amortized methods as the number of groups becomes larger.

### 3.3 Experiment 3: Style inference for hand-drawn digits

As a final experiment, we demonstrate the efficacy of our amortized multilevel approximator on unstructured, high-dimensional observations. Concretely, the observations  $\mathbf{x}$  are images that are generated from a pre-trained generative neural network which we treat as a black-box simulator (i.e., an implicit data model), see Figure 10 for an overview.

The simulator is a general incompressible flow network (GIN; Sorrenson et al., 2020) which has been trained on the digits of the EMNIST data set (Cohen et al., 2017). The GIN learns a class-conditional bijective mapping from the image domain to a disentangled latent space, which can be interpreted as a nonlinear independent component analysis (ICA). We treat the decoder of the pre-trained GIN as the “likelihood” which is parameterized by the 4 dimensions with the highest variance of the latent space. These parameters encode global style features across all digits (see Sorrenson et al., 2020, for a detailed analysis). Additionally, we condition the decoder on random noise variates  $\nu$  to induce aleatoric uncertainty in the learned bijective mapping of the GIN. We use ABI to approximate the posterior over the latent “style” variables of the GIN simulator.

Our multi-level setting features ten subjects  $j = 1, \dots, 10$ . Each subject has a 4-dimensional style vector  $\theta_j = (\theta_{j,1}, \dots, \theta_{j,4})$ , and the entirety of these styles constitute the local parameters  $\theta \in \mathbb{R}^{10 \times 4}$ . The global parameters are an average style  $\mu \in \mathbb{R}^4$ , the style dispersion  $\sigma \in \mathbb{R}_{>0}^4$ , and the 6 unique elements of a correlation matrix  $\Omega \in [-1, 1]^{4 \times 4}$  between style dimensions. The forward simulation program is formalized as

$$\begin{aligned}
 \mu &\sim \text{Normal}(\mathbf{0}, 0.3 \cdot \mathbf{I}), \quad \sigma \sim \text{Exponential}(5), \quad \Omega \sim \text{LKJ}(2), && \text{(global parameters)} \\
 \theta_j &\sim \text{Normal}(\mu, \Sigma) \quad \text{with } \Sigma = \text{diag}(\sigma) \Omega \text{diag}(\sigma) \text{ and } j = 1, \dots, J, && \text{(local parameters)} \\
 \mathbf{x}_j &= \text{GIN}(\theta_j, \nu) \text{ with } j = 1, \dots, J, && \text{(data model)}
 \end{aligned} \tag{24}$$

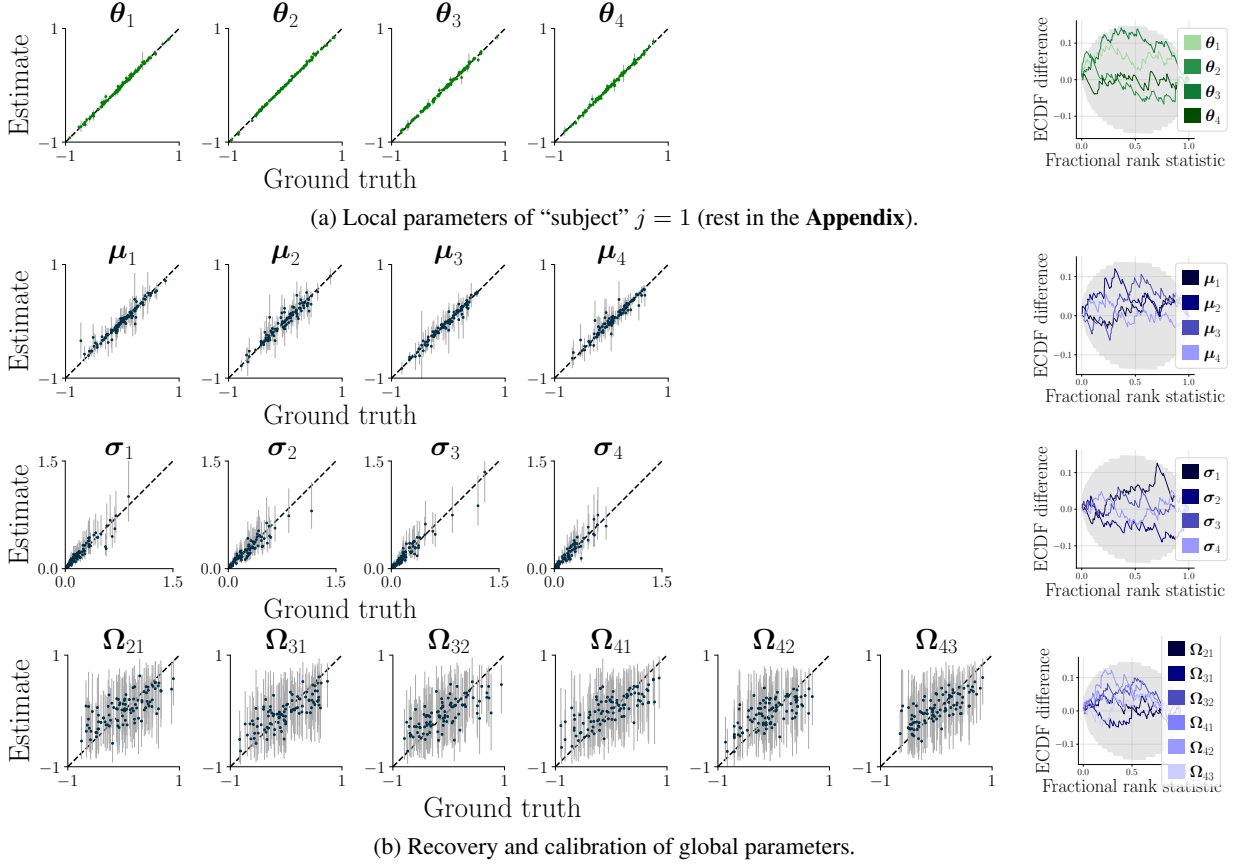


Figure 11: **Experiment 3**. The recovery of the local parameters (a, left) and global parameters (b, left) is at the upper limit given the epistemic and aleatoric uncertainty in the probabilistic model. Dots indicate posterior means, vertical bars represent the symmetric 95% posterior credible intervals. All local and global parameters are well-calibrated (right, SBC-ECDF plots).

where  $\text{Normal}(\boldsymbol{\mu}, \boldsymbol{\Sigma})$  is a multivariate normal distribution with mean  $\boldsymbol{\mu}$  and covariance  $\boldsymbol{\Sigma}$ ,  $\mathbf{I}$  is the  $4 \times 4$  identity matrix,  $\text{Exponential}(\lambda)$  is an exponential distribution with rate  $\lambda$ ,  $\text{LKJ}(\gamma)$  is the Lewandowski-Kurowicka-Joe distribution with shape  $\gamma$ , and  $\text{GIN} : (\boldsymbol{\theta}_j, \boldsymbol{\nu}) \mapsto \mathbf{x}_j$  is the decoder of the pre-trained global incompressible-flow network from [Sorrenson et al. \(2020\)](#) with style vector  $\boldsymbol{\theta}_j$  and unmodeled nuisance parameters  $\boldsymbol{\nu}$ .

**Model training** The global summary network  $h_{\psi_1}$  is a set transformer ([Lee et al., 2019](#)) which learns a 32-dimensional embedding from the local summary vectors of all subjects (see below). The local summary network  $h_{\psi_2}$  extracts 32 features from each subject’s  $28 \times 28$  image through a sequence of residual convolutional blocks followed by average pooling. Both the global inference network  $f_{\phi_1}$  and the local inference network  $f_{\phi_2}$  are affine coupling flows. The **Appendix** contains details about the neural networks and training hyperparameters.

**Results** We draw 1000 approximate posterior samples from our amortized neural estimators and report the recovery and calibration of local and global parameters in the following. The approximate posteriors for the global parameters  $\boldsymbol{\mu}, \boldsymbol{\sigma}, \boldsymbol{\Omega}$  show excellent calibration (see [Figure 11b](#)). While the ground-truths of the average style  $\boldsymbol{\mu}$  dispersion  $\boldsymbol{\sigma}$  can be recovered with near-perfect accuracy, the recovery of the global correlation matrix  $\boldsymbol{\Omega}$  is bounded due to the limited sample size of  $J = 10$  subjects. All local parameters of all subjects can be recovered with excellent precision and satisfactory calibration (SBC; see [Figure 11a](#) and [Figure 13](#)). This experiment underscores the scalability of our amortized multilevel approximator to high data dimensions, correlated parameters, and black-box forward simulators.



## 4 Conclusion

In this paper, we developed a framework for amortized Bayesian inference of multilevel models using deep generative neural networks. By exploiting the probabilistic symmetries of multilevel models and mirroring them in the neural architectures, we not only enable efficient training of the neural approximators but also flexible amortization over both the number of groups and the number of observations within groups. This means that, once trained, our neural approximators provide near instant inference of the multilevel model on any number of new datasets or data subsets. We extensively studied our framework in three realistic case studies, where we demonstrate both the amortization capabilities and the accuracy of the resulting Bayesian inference as validated by simulation-based calibration and comparison with Stan where possible. To foster practical application, we implemented our methods and architectures in the Python library Bayesflow (Radev et al., 2023b), which provides efficient and user-friendly workflows for amortized Bayesian inference.

### 4.1 Future Work

So far, research on amortized multilevel modeling has focused on two-level models only. This already covers a lot of use cases, but still leaves out many practically scenarios of inference on datasets with more than two levels, which should be considered in future work. Another challenge is presented by models with very expensive simulators, such that only very few (say, a maximum of a couple of hundred) simulations are available for training the neural approximators. In this low data regime, fully amortized methods may not achieve acceptable levels of inference accuracy and calibrations (Lueckmann et al., 2021; Schmitt et al., 2024a; Radev et al., 2023a; Geffner et al., 2023). Instead, sequential neural methods, which enable targeted inference only for a single dataset (Papamakarios and Murray, 2016; Greenberg et al., 2019), may be better suited but have yet to be developed for multilevel models.

## Acknowledgments

Daniel Habermann, Lars Kühmichel, Stefan Radev, and Paul Bürkner acknowledge support of the Deutsche Forschungsgemeinschaft (DFG, German Research Foundation) Projects 508399956 and 528702768. Marvin Schmitt and Paul Bürkner acknowledge support of Cyber Valley Project CyVy-RF- 2021-16, the DFG under Germany’s Excellence Strategy – EXC-2075 - 390740016 (the Stuttgart Cluster of Excellence SimTech). Marvin Schmitt acknowledges travel support from the European Union’s Horizon 2020 research and innovation programme under grant agreements No 951847 (ELISE) and No 101070617 (ELSA), and the Aalto Science-IT project.

## References

- Agarap, A. F. (2018). “Deep Learning using Rectified Linear Units (ReLU).” *arXiv preprint*. 9
- Alexanderson, S. and Henter, G. E. (2020). “Robust model training and generalisation with Studentising flows.” *arXiv preprint*. 6
- Ardizzone, L., Kruse, J., Wirkert, S., Rahner, D., Pellegrini, E. W., Klessen, R. S., Maier-Hein, L., Rother, C., and Köthe, U. (2018). “Analyzing inverse problems with invertible neural networks.” *arXiv preprint*. 5
- Ardizzone, L., Lüth, C., Kruse, J., Rother, C., and Köthe, U. (2019). “Guided image generation with conditional invertible neural networks.” *arXiv preprint*. 5, 8
- Arruda, J., Schälte, Y., Peiter, C., Teplytska, O., Jaehde, U., and Hasenauer, J. (2023). “An amortized approach to non-linear mixed-effects modeling based on neural posterior estimation.” *bioRxiv*. 3
- Avecilla, G., Chuong, J. N., Li, F., Sherlock, G., Gresham, D., and Ram, Y. (2022). “Neural networks enable efficient and accurate simulation-based inference of evolutionary parameters from adaptation dynamics.” *PLoS biology*, 20(5): e3001633. 5
- Barber, S., Voss, J., and Webster, M. (2015). “The rate of convergence for approximate Bayesian computation.” *Electronic Journal of Statistics*, 9(1). 2
- Bieringer, S., Butter, A., Heimel, T., Höche, S., Köthe, U., Plehn, T., and Radev, S. T. (2021). “Measuring QCD splittings with invertible networks.” *SciPost Physics*, 10(6): 126. 5
- Brehmer, J., Louppe, G., Pavez, J., and Cranmer, K. (2020). “Mining gold from implicit models to improve likelihood-free inference.” *Proceedings of the National Academy of Sciences*, 117(10): 5242–5249. 2
- Bürkner, P.-C. (2021). “Bayesian Item Response Modeling in R with brms and Stan.” *Journal of Statistical Software*, 100(5): 1–54. 2

- Chen, Y., Zhang, D., Gutmann, M., Courville, A., and Zhu, Z. (2020). “Neural approximate sufficient statistics for implicit models.” *arXiv preprint*. 6
- Cohen, G., Afshar, S., Tapson, J., and Van Schaik, A. (2017). “EMNIST: Extending MNIST to handwritten letters.” In *2017 international joint conference on neural networks (IJCNN)*, 2921–2926. IEEE. 17
- Cranmer, K., Brehmer, J., and Louppe, G. (2020). “The frontier of simulation-based inference.” *Proceedings of the National Academy of Sciences*, 117(48): 30055–30062. 1, 2, 4
- Diggle, P. J. and Gratton, R. J. (1984). “Monte Carlo methods of inference for implicit statistical models.” *Journal of the Royal Statistical Society Series B: Statistical Methodology*, 46(2): 193–212. 4
- Durkan, C., Bekasov, A., Murray, I., and Papamakarios, G. (2019). “Neural Spline Flows.” *arXiv preprint*. 9
- Eurostat (2022a). “Household debt, consolidated including Non-profit institutions serving households - % of GDP.” 9, 10
- (2022b). “International extra-EU air passenger transport by reporting country and partner world regions and countries.” 9, 10
- (2022c). “Real GDP per capita.” 9, 10
- Finch, W. H., Bolin, J. E., and Kelley, K. (2019). *Multilevel modeling using R*. Chapman and Hall/CRC. 1
- Geffner, T., Papamakarios, G., and Mnih, A. (2023). “Compositional Score Modeling for Simulation-Based Inference.” In Krause, A., Brunskill, E., Cho, K., Engelhardt, B., Sabato, S., and Scarlett, J. (eds.), *Proceedings of the 40th International Conference on Machine Learning*, volume 202 of *Proceedings of Machine Learning Research*, 11098–11116. PMLR. 19
- Gelfand, A. E. (2000). “Gibbs sampling.” *Journal of the American Statistical Association*, 95(452): 1300–1304. 4
- Gelman, A. (2006). “Multilevel (Hierarchical) Modeling: What It Can and Cannot Do.” *Technometrics*, 48(3): 432–435. 3
- Gelman, A., Carlin, J. B., Stern, H. S., Dunson, D. B., Vehtari, A., and Rubin, D. B. (2013). *Bayesian Data Analysis*. Chapman and Hall/CRC. 1
- Gelman, A. and Hill, J. (2006). *Data Analysis Using Regression and Multilevel/Hierarchical Models*. Cambridge University Press. 1, 2, 12
- Gelman, A., Vehtari, A., Simpson, D., Margossian, C. C., Carpenter, B., Yao, Y., Kennedy, L., Gabry, J., Bürkner, P.-C., and Modrák, M. (2020). “Bayesian Workflow.” *arXiv preprint*. 2, 4, 14
- Gershman, S. and Goodman, N. (2014). “Amortized inference in probabilistic reasoning.” In *Proceedings of the annual meeting of the cognitive science society*, volume 36. 2, 4
- Gloeckler, M., Deistler, M., Weilbach, C., Wood, F., and Macke, J. H. (2024). “All-in-one simulation-based inference.” *arXiv preprint*. 5
- Glorot, X. and Bengio, Y. (2010). “Understanding the difficulty of training deep feedforward neural networks.” In Teh, Y. W. and Titterton, M. (eds.), *Proceedings of the Thirteenth International Conference on Artificial Intelligence and Statistics*, volume 9 of *Proceedings of Machine Learning Research*, 249–256. Chia Laguna Resort, Sardinia, Italy: PMLR. 14
- Goldstein, H. (2011). *Multilevel statistical models*. John Wiley & Sons. 1
- Gonçalves, P. J., Lueckmann, J.-M., Deistler, M., Nonnenmacher, M., Öcal, K., Bassetto, G., Chintaluri, C., Podlaski, W. F., Haddad, S. A., Vogels, T. P., et al. (2020). “Training deep neural density estimators to identify mechanistic models of neural dynamics.” *Elife*, 9: e56261. 2, 5
- Greenberg, D., Nonnenmacher, M., and Macke, J. (2019). “Automatic Posterior Transformation for Likelihood-Free Inference.” In *Proceedings of the 36th International Conference on Machine Learning*, 2404–2414. PMLR. ISSN: 2640-3498. 19
- Heinrich, L., Mishra-Sharma, S., Pollard, C., and Windischhofer, P. (2023). “Hierarchical Neural Simulation-Based Inference Over Event Ensembles.” 3, 6
- Hochreiter, S. and Schmidhuber, J. (1997). “Long Short-Term Memory.” *Neural Computation*, 9(8): 1735–1780. 9
- Hoffman, M., Sountsov, P., Dillon, J. V., Langmore, I., Tran, D., and Vasudevan, S. (2019). “Neutralizing Bad Geometry in Hamiltonian Monte Carlo Using Neural Transport.” *arXiv preprint*. 2
- Huang, D., Bharti, A., Souza, A., Acerbi, L., and Kaski, S. (2024). “Learning robust statistics for simulation-based inference under model misspecification.” *Advances in Neural Information Processing Systems*, 36. 5

- Kingma, D. P. and Ba, J. (2014). “Adam: A Method for Stochastic Optimization.” *arXiv preprint*. 9
- Kobyzev, I., Prince, S. J., and Brubaker, M. A. (2020). “Normalizing flows: An introduction and review of current methods.” *IEEE Transactions on Pattern Analysis and Machine Intelligence*, 43(11): 3964–3979. 5
- Kruse, J., Ardizzone, L., Rother, C., and Köthe, U. (2021). “Benchmarking invertible architectures on inverse problems.” *arXiv preprint*. 5
- Lavin, A., Krakauer, D., Zenil, H., Gottschlich, J., Mattson, T., Brehmer, J., Anandkumar, A., Choudry, S., Rocki, K., Baydin, A. G., et al. (2021). “Simulation intelligence: Towards a new generation of scientific methods.” *arXiv preprint*. 4
- Le, T. A., Baydin, A. G., and Wood, F. (2017). “Inference compilation and universal probabilistic programming.” In *Artificial Intelligence and Statistics*, 1338–1348. PMLR. 4
- Lee, J., Lee, Y., Kim, J., Kosiorek, A., Choi, S., and Teh, Y. W. (2019). “Set Transformer: A Framework for Attention-based Permutation-Invariant Neural Networks.” In *Proceedings of the 36th International Conference on Machine Learning*, 3744–3753. 18
- Lee, J., Lee, Y., Kim, J., Kosiorek, A. R., Choi, S., and Teh, Y. W. (2018). “Set Transformer: A Framework for Attention-based Permutation-Invariant Neural Networks.” *arXiv preprint*. 9
- Loshchilov, I. and Hutter, F. (2016). “SGDR: Stochastic Gradient Descent with Warm Restarts.” *arXiv preprint*. 9
- Lueckmann, J.-M., Boelts, J., Greenberg, D., Goncalves, P., and Macke, J. (2021). “Benchmarking Simulation-Based Inference.” In Banerjee, A. and Fukumizu, K. (eds.), *Proceedings of The 24th International Conference on Artificial Intelligence and Statistics*, volume 130 of *Proceedings of Machine Learning Research*, 343–351. PMLR. 19
- Margossian, C. C., Hoffman, M. D., Sountsov, P., Riou-Durand, L., Vehtari, A., and Gelman, A. (2021). “Nested  $\hat{R}$ : Assessing the convergence of Markov chain Monte Carlo when running many short chains.” *arXiv preprint*. 2
- McGlothlin, A. E. and Viele, K. (2018). “Bayesian hierarchical models.” *JAMA*, 320(22): 2365–2366. 1
- Merkle, E. C., Furr, D., and Rabe-Hesketh, S. (2019). “Bayesian Comparison of Latent Variable Models: Conditional Versus Marginal Likelihoods.” *Psychometrika*, 84(3): 802–829. 2, 14
- Modi, C., Barnett, A., and Carpenter, B. (2023). “Delayed rejection Hamiltonian Monte Carlo for sampling multiscale distributions.” *Bayesian Analysis*, 1–28. 2
- Modrák, M., Moon, A. H., Kim, S., Bürkner, P., Huurre, N., Faltejsková, K., Gelman, A., and Vehtari, A. (2023). “Simulation-based calibration checking for Bayesian computation: The choice of test quantities shapes sensitivity.” *Bayesian Analysis*, 1(1): 1–28. 2
- Neal, R. M. (2011). “MCMC Using Hamiltonian Dynamics.” In *Handbook of Markov Chain Monte Carlo*, 113–162. Chapman and Hall/CRC. 4
- Papamakarios, G. and Murray, I. (2016). “Fast  $\epsilon$ -free Inference of Simulation Models with Bayesian Conditional Density Estimation.” In *Advances in Neural Information Processing Systems*, volume 29. Curran Associates, Inc. 2, 19
- Piironen, J. and Vehtari, A. (2017). “Sparsity information and regularization in the horseshoe and other shrinkage priors.” *Electronic Journal of Statistics*, 11(2): 5018–5051. Publisher: The Institute of Mathematical Statistics and the Bernoulli Society. 2
- Radev, S. T., Graw, F., Chen, S., Mutters, N. T., Eichel, V. M., Bärnighausen, T., and Köthe, U. (2021). “OutbreakFlow: Model-based Bayesian inference of disease outbreak dynamics with invertible neural networks and its application to the COVID-19 pandemics in Germany.” *PLoS computational biology*, 17(10): e1009472. 2
- Radev, S. T., Mertens, U. K., Voss, A., Ardizzone, L., and Kothe, U. (2020). “BayesFlow: Learning Complex Stochastic Models With Invertible Neural Networks.” *IEEE Transactions on Neural Networks and Learning Systems*, 33(4): 1452–1466. 2, 4, 5, 6
- Radev, S. T., Schmitt, M., Pratz, V., Picchini, U., Köthe, U., and Bürkner, P.-C. (2023a). “JANA: Jointly Amortized Neural Approximation of Complex Bayesian Models.” In Evans, R. J. and Shpitser, I. (eds.), *Proceedings of the 39th Conference on Uncertainty in Artificial Intelligence*, volume 216 of *Proceedings of Machine Learning Research*, 1695–1706. PMLR. 19
- Radev, S. T., Schmitt, M., Schumacher, L., Elsemüller, L., Pratz, V., Schälte, Y., Köthe, U., and Bürkner, P.-C. (2023b). “BayesFlow: Amortized Bayesian Workflows With Neural Networks.” *Journal of Open Source Software*, 8(89): 5702. 3, 8, 19
- Ratcliff, R., Smith, P. L., Brown, S. D., and McKoon, G. (2016). “Diffusion decision model: Current issues and history.” *Trends in cognitive sciences*, 20(4): 260–281. 13

- Ritchie, D., Horsfall, P., and Goodman, N. D. (2016). “Deep amortized inference for probabilistic programs.” *arXiv preprint*. 4
- Robert, C. P. et al. (2007). *The Bayesian choice: from decision-theoretic foundations to computational implementation*, volume 2. Springer. 3
- Rodrigues, P. L. C., Moreau, T., Louppe, G., and Gramfort, A. (2021). “HNPE: Leveraging Global Parameters for Neural Posterior Estimation.” 3
- Roeder, G., Grant, P., Phillips, A., Dalchau, N., and Meeds, E. (2019). “Efficient amortised bayesian inference for hierarchical and nonlinear dynamical systems.” In *International Conference on Machine Learning*, 4445–4455. PMLR. 2
- Schmitt, M., Bürkner, P.-C., Köthe, U., and Radev, S. T. (2022). “Detecting Model Misspecification in Amortized Bayesian Inference with Neural Networks.” 5
- Schmitt, M., Habermann, D., Köthe, U., Bürkner, P.-C., and Radev, S. T. (2024a). “Leveraging Self-Consistency for Data-Efficient Amortized Bayesian Inference.” *Proceedings of the International Conference on Machine Learning (ICML)*. 19
- Schmitt, M., Pratz, V., Köthe, U., Bürkner, P.-C., and Radev, S. T. (2024b). “Consistency Models for Scalable and Fast Simulation-Based Inference.” *arXiv preprint*. 5
- Sharrock, L., Simons, J., Liu, S., and Beaumont, M. (2022). “Sequential Neural Score Estimation: Likelihood-Free Inference with Conditional Score Based Diffusion Models.” 5
- Sisson, S. A. and Fan, Y. (2011). “Likelihood-free MCMC.” *Handbook of Markov Chain Monte Carlo*, 313–335. 2
- Sisson, S. A., Fan, Y., and Beaumont, M. A. (2018). “Overview of ABC.” 2
- Sorrenson, P., Rother, C., and Köthe, U. (2020). “Disentanglement by Nonlinear ICA with General Incompressible-flow Networks (GIN).” In *International Conference on Learning Representations*. 17, 18
- Stan Development Team (2024). “Stan Modeling Language Users Guide and Reference Manual, 2.31.0.” URL <https://mc-stan.org> 2
- Steele, F. (2008). “Multilevel models for longitudinal data.” *Journal of the Royal Statistical Society Series A: Statistics in Society*, 171(1): 5–19. 2
- Stuhlmüller, A., Taylor, J., and Goodman, N. (2013). “Learning stochastic inverses.” *Advances in neural information processing systems*, 26. 4
- Talts, S., Betancourt, M., Simpson, D., Vehtari, A., and Gelman, A. (2018). “Validating Bayesian Inference Algorithms with Simulation-Based Calibration.” *arXiv preprint*. 2, 4, 14
- Tran, D., Ranganath, R., and Blei, D. (2017). “Hierarchical implicit models and likelihood-free variational inference.” *Advances in Neural Information Processing Systems*, 30. 2
- Vehtari, A., Gelman, A., and Gabry, J. (2017). “Practical Bayesian model evaluation using leave-one-out cross-validation and WAIC.” *Statistics and Computing*, 27(5): 1413–1432. 2, 4, 14, 17
- Vehtari, A., Simpson, D., Gelman, A., Yao, Y., and Gabry, J. (2024). “Pareto Smoothed Importance Sampling.” *Journal of Machine Learning Research*, 25(72): 1–58. 14
- von Krause, M., Radev, S. T., and Voss, A. (2022). “Mental speed is high until age 60 as revealed by analysis of over a million participants.” *Nature human behaviour*, 6(5): 700–708. 2, 4, 5
- Wagenmakers, E.-J., Ratcliff, R., Gomez, P., and McKoon, G. (2008). “A diffusion model account of criterion shifts in the lexical decision task.” *Journal of Memory and Language*, 58(1): 140–159. 14, 16
- Wehenkel, A., Behrmann, J., Miller, A. C., Sapiro, G., Sener, O., Cuturi, M., and Jacobsen, J.-H. (2023). “Simulation-based inference for cardiovascular models.” *arXiv preprint*. 2
- Wildberger, J., Dax, M., Buchholz, S., Green, S., Macke, J. H., and Schölkopf, B. (2024). “Flow Matching for Scalable Simulation-Based Inference.” *Advances in Neural Information Processing Systems*, 36. 5
- Yao, Y., Pirš, G., Vehtari, A., and Gelman, A. (2022). “Bayesian hierarchical stacking: Some models are (somewhere) useful.” *Bayesian Analysis*, 17(4): 1043–1071. 1
- Yao, Y., Vehtari, A., Simpson, D., and Gelman, A. (2018). “Yes, but Did It Work?: Evaluating Variational Inference.” In *Proceedings of the 35th International Conference on Machine Learning*, 5581–5590. PMLR. ISSN: 2640-3498. 2
- Zhang, L., Carpenter, B., Gelman, A., and Vehtari, A. (2022). “Pathfinder: Parallel quasi-Newton variational inference.” *Journal of Machine Learning Research*, 23(306): 1–49. 2
- Zhang, Y. and Mikelsons, L. (2023). “Solving stochastic inverse problems with stochastic bayesflow.” In *2023 IEEE/ASME International Conference on Advanced Intelligent Mechatronics (AIM)*, 966–972. IEEE. 2

## A Experiment 2: Varying simulation budgets

To better understand the relationship between simulation budget and quality of posterior inference, we refit the diffusion decision model with network training budgets of 1000, 2000, 5000, 10000 and 20000 simulated datasets. For each of these models, we quantify posterior fidelity by computing the maximum mean discrepancy (MMD) between the posterior conditioned on the experimental data described in paragraph [Posterior inference](#) and the results obtained by Stan ([Figure 12](#)).

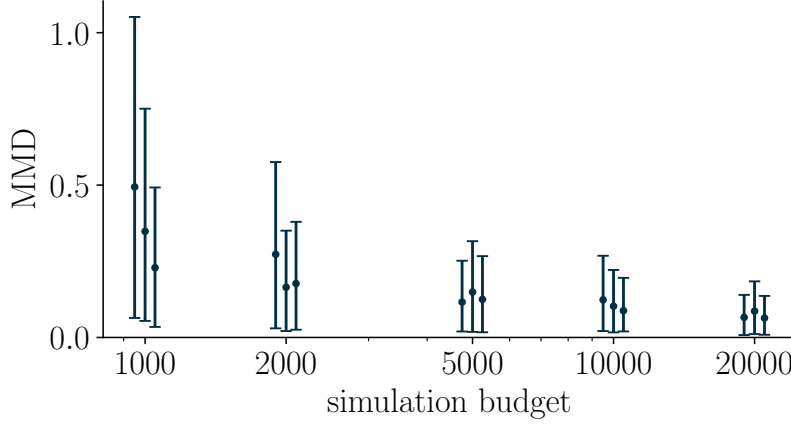


Figure 12: MMD between the posterior obtained by ML-NPE on experimental data and a reference posterior obtained by fitting the same model in Stan. For each simulation budget, we repeat model fitting three times on different training data. Errorbars show 95% confidence intervals quantifying variation in MMD between the 21 trial blocks.

## B Experiment 3: Details

The global inference network is an affine coupling flow with 6 coupling layers, each of which features 2 dense layers with 128 units, 5% dropout, and kernel regularization with strength  $10^{-4}$ . The local inference network is an affine coupling flow with 10 coupling layers, each of which features one dense layer with 512 units, no dropout, and kernel regularization with strength  $10^{-4}$ . The local summary network is a convolutional neural network (CNN) with residual connections, Mish activation, and He Normal initialization, followed by average pooling. The filter sizes of the convolutional layers are 32–64–32–32–32(output). The global summary network is a set transformer with 32 output dimensions, 32 inducing points, 2 dense layers, and 2 attention blocks. The neural networks are trained for 200 epochs with a batch size of 128 and 500 iterations per epoch. We use the Adam optimizer with an initial learning rate of  $10^{-3}$  and cosine decay.



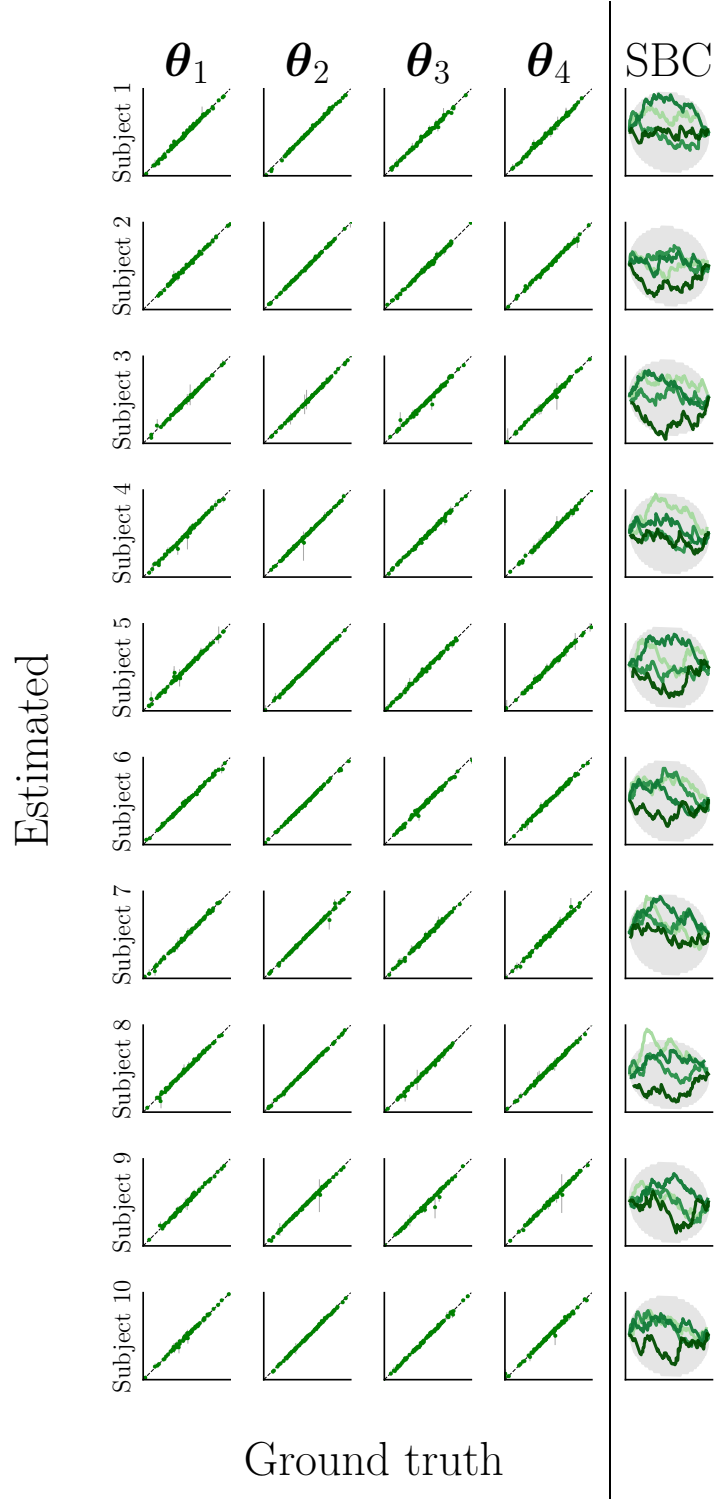


Figure 13: **Experiment 3.** Our amortized multilevel approximator shows excellent recovery and satisfactory simulation-based calibration for all parameters and subjects. The main text shows the results of subject 1 (Figure 11a).